Am J Cancer Res 2023;13(11):5174-5196
www.ajcr.us /ISSN:2156-6976/ajcr0152191

Original Article

NR0B1 suppresses ferroptosis through upregulation of NRF2/c-JUN-CBS signaling pathway in lung cancer cells

Xin-Yue Zhang[1*], Hao Zhang[1,2*], Si-Jing Hu[3*], Shun-Yao Liao[3*], Da-Chang Tao[1], Xiao-Lan Tan[1], Ming Yi[1], Xiang-You Leng[1], Zhao-Kun Wang[1], Jia-Ying Shi[1], Sheng-Yu Xie[1], Yuan Yang[1], Yun-Qiang Liu[1]

[1]Department of Medical Genetics and State Key Laboratory of Biotherapy, West China Hospital, Sichuan University, Chengdu 610041, Sichuan, China; [2]Department of Pathology and Infectious Diseases, People's Hospital of Deyang City, Deyang 618000, Sichuan, China; [3]Institute of Gerontology and Center for Geriatrics, Sichuan Academy of Medical Sciences and Sichuan Provincial People's Hospital, University of Electronic Science and Technology of China, Chengdu 610071, Sichuan, China. [*]Equal contributors.

Received July 13, 2023; Accepted October 25, 2023; Epub November 15, 2023; Published November 30, 2023

Abstract: Ferroptosis has demonstrated significant potential in treating radiochemotherapy-resistant cancers, but its efficacy can be affected by recently discovered ferroptosis suppressors. In this study, we discovered that NR0B1 protects against erastin- or RSL3-induced ferroptosis in lung cancer cells. Transcriptomic analysis revealed that NR0B1 significantly interfered with the expression of 12 ferroptosis-related genes, and the expression level of NR0B1 positively correlated with that of c-JUN, NRF2, and CBS. We further revealed that NR0B1 suppression of ferroptosis depended on the activities of c-JUN, NRF2, and CBS. NR0B1 directly promoted the expression of NRF2 and c-JUN and indirectly upregulated CBS expression through enhancing NRF2 and/or c-JUN transcription. Moreover, we showed that NR0B1 depletion restrained xenograft tumor growth and facilitated RSL3-induced ferroptosis in the tumors. In conclusion, our findings uncover that NR0B1 suppresses ferroptosis by activating the c-JUN/NRF2-CBS signaling pathway in lung cancer cells, providing new evidence for the involvement of NR0B1 in drug resistance during cancer therapy.

Keywords: NR0B1, ferroptosis, CBS, NRF2, c-JUN, lung cancer, drug resistance

Introduction

Lung cancer is the most prevalent malignant cancer worldwide [1]. Despite advancements in surgical techniques, chemotherapeutic agents, molecularly targeted drugs, and immunotherapeutic antibodies, a substantial number of patients succumb due to recurrence and treatment failure. Currently, lung cancer remains the leading global cause of cancer-related death. To a certain extent, drug resistance invariably leads to treatment failure [2]. Consequently, ongoing studies on the mechanisms of drug resistance are pivotal for lung cancer treatment.

Ferroptosis, a newly identified iron-dependent form of regulated cell death (RCD), is characterized by an increased intracellular iron level, accumulation of lipid peroxidation products (such as malondialdehyde (MDA)), reactive oxygen species (ROS), and decreased intracellular levels of glutathione (GSH) [3]. ROS and lipid oxidation are often produced in cancer cells under radiation or chemical treatment. Therefore, ferroptosis has been implicated in numerous types of cancers and has become a research focal point for treating various cancers, including lung cancer [3, 4]. In particular, numerous chemicals have been reported to induce ferroptosis in lung cancer through various targets [5-7]. Simultaneously, several genes, including *NFS1* (encoding an iron-sulfur cluster biosynthetic enzyme) [8], *SOX2* [9], *RBMS1* [10], *TP53* [11], *P53RRA* [12] and *LINC00336* [13], have been shown to inhibit ferroptosis in lung cancer. Given the complexity of the regulatory mechanisms of ferroptosis, further investigation into the mechanisms of ferroptosis suppressors is necessary before utilizing ferroptosis-based therapy.

NR0B1 (*nuclear receptor subfamily 0 group B member 1*), also known as *DAX1* (*dosage-sensitive sex reversal-AHC critical region on the X-chromosome gene 1*), is typically expressed in the reproductive and endocrine systems and encodes an unusual orphan nuclear receptor, exhibiting significant evolutionary conservation from fish to mammals [14]. Through interactions with OCT4 [15], SOX2 [16] and NANOG [17], NR0B1 participates in the transcriptional network, maintaining the pluripotency of embryonic stem cells. The duplication of NR0B1 leads to male-to-female sex reversal [18], and point mutations commonly result in both X-linked congenital adrenal hypoplasia and hypogonadotropic hypogonadism [19]. Notably, NR0B1 is often ectopically expressed in many cancers such as Ewing's tumor [20], breast cancer [21], cervical cancer [22], ovarian carcinoma [23], prostate cancer [24], and lung cancer [25, 26]. Investigations, including ours, have revealed that NR0B1 plays roles in maintaining stem cell characteristics and resisting drug effects in lung cancer [25, 26]. However, the detailed mechanism of NR0B1-mediated chemical resistance remains unclear.

Cysteine metabolism is a key event pathway in regulating cell ferroptosis [27, 28]. Recently, researchers globally mapped cysteine reactivity in lung cancer cells through chemical proteomics [29]. They found that a rich content of cysteines is amenable to modification and uncovered that NR0B1 is involved in the modification through forming a multimeric transcriptional complex for regulating the expression of NRF2 (nuclear factor erythroid 2-related factor 2)-targeted genes. Concurrently, NRF2 is a key regulator for antioxidant response [30] and ferroptosis-resistance [31]. Thus, it merits investigation into whether and how NR0B1 is involved in ferroptosis to influence drug resistance. Our present study revealed that NR0B1 significantly suppressed erastin- or RSL3-induced ferroptosis in lung cancer cells. NR0B1 transcriptionally elevates the expression of c-JUN and NRF2, which further upregulate the activity of cystathionine beta-synthase (CBS) to alleviate cell ferroptosis.

Materials and methods

Plasmid construction

Full-length cDNA encoding AM-tagged NR0B1, NRF2, and c-JUN were separately synthesized and cloned into lentiviral vectors: pEZ-Lv201, pEZ-Lv152, and pEZ-Lv151 (GeneCopoeia Inc., Rockville, MD), respectively. Specific shRNAs targeting NR0B1 (shNR0B1) and NRF2 (shNRF2) were synthesized and inserted into vectors psi-LVRU6GP and psi-LVRU6GH (GeneCopoeia Inc.), respectively. c-JUN-specific shRNA (sh c-JUN) was synthesized and inserted into the pGV117 vector (Genechem, Shanghai, China). CBS-specific siRNA (siCBS) was synthesized by RIBOBIO (Guangzhou, China). The mutant NR0B1 coding sequence, carrying an eleven-nt mismatch to the shNR0B1 sequence, was synthesized and inserted into the pEZ-Lv201 vector to rescue NR0B1 expression. The sequences of the above constructions are listed in Table S1.

Promoter fragments of various lengths from NRF2, c-JUN, and CBS were amplified (primers are listed in Table S2) and cloned into the pGL3-Basic luciferase reporter vector (Promega, Madison, WI).

Cell culture and transient transfection

Six lung cancer cell lines, including A549, H1437, H460, H1299, H1975, and H838, were purchased from the Shanghai Institute of Biochemistry and Cell Biology (Shanghai, China). All cell lines were authenticated by short tandem repeat (STR) profiling and tested for mycoplasma contamination using a PCR-based method. Cells were cultured in RPMI-1640 medium supplemented with 10% fetal bovine serum (Gemini, Woodland, CA) and incubated in a humidified atmosphere with 5% CO_2 at 37°C. Cells were plated 24 hours before transfection and then transiently transfected using ExFect2000 (Vazyme, Nanjing, China) according to the manufacturer's instructions.

Lentivirus transduction

Lentiviral particles were produced by GeneCopoeia Inc. For infection, cells were plated in 12-well plates. Once cells reached 30-40% confluency, 2 μL of each lentivirus was added to the culture medium and incubated at 37°C for 24 hours. Subsequently, stable cell lines with altered expression levels of NR0B1, NRF2, and c-JUN were selected using a selection culture medium containing 2 μg/ml puromycin, 400 μg/ml hygromycin, or 600 μg/ml neomycin.

Cell viability assay

Cell viability was assessed in a 96-well format using the CellTiter 96 Aqueous One Solution Cell Proliferation Assay (Promega, Madison, WI). Briefly, 2 × 10^3 cells were seeded per well in 96-well plates and allowed to adhere for 24 hours. Following treatment with various concentrations of Erastin or RSL3 (Selleck Chemicals, Houston, TX), CellTiter96® Aqueous One Solution (20 μl/well) was added, and cell viability was measured at 490 nm using a Synergy™Mx microplate reader.

MDA assay

The relative MDA concentration was assessed using an MDA Assay kit (Abcam, Cambridge, UK) per the manufacturer's instructions. Briefly, free MDA in the treated cells reacted with thiobarbituric acid (TBA), generating an MDA-TBA adduct, the concentration of which was determined by quantifying optical density (OD) at 532 nm.

Iron assay

Intracellular iron levels were measured using an Iron Assay kit (Abcam) according to the manufacturer's instructions. Briefly, samples were collected and washed three times with cold PBS. Samples were then homogenized in 5 volumes of iron assay buffer on ice using a Dounce homogenizer. After centrifugation at 16,000 g for 10 min, the supernatant was collected, and an iron reducer was added to each sample prior to mixing. Following a 30-min incubation, the iron probe was added to each sample and mixed, then incubated for an additional 60 min. The output was immediately measured on a colorimetric microplate reader (Synergy™Mx, OD = 593 nm).

ROS assay

ROS levels were determined using CellROX® Oxidative Stress Reagents (Life Technologies, Carlsbad, CA), according to the manufacturer's instructions. Briefly, cells were seeded in six-well plates and cultured for 24 hours. After a 24-hour incubation with indicated concentrations of RSL3, the culture medium was replaced with 2 ml of culture medium containing 5 μM of CellROX® Deep Red Reagent, and cells were cultured at 37°C for 30 min. Subsequently, cells were harvested, washed thrice with PBS, and resuspended in 500 μl of PBS. The fluorescence intensities of the cells were determined by a colorimetric microplate reader (Synergy™Mx).

Glutathione assay

Intracellular levels of glutathione were assayed using a Glutathione Assay Kit (Sigma-Aldrich, St. Louis, MO). Harvested cells were first deproteinized with the 5-Sulfosalicylic acid solution and then successively reacted with the working solution containing assay buffer, diluted enzyme, and 5,5-Dithiobis (2-nitrobenzoic acid), as well as the diluted NADPH solution. The output was measured immediately on a colorimetric microplate reader (Synergy™Mx) (OD = 412 nm) using a kinetic model.

RNA-Seq and transcriptomic analysis

Total RNA was respectively isolated from the NR0B1-KD A549 cells and the control cells using TRIzol reagent (Life Technologies, Carlsbad, CA). After measuring the quality and concentration of total RNA using an Agilent 2100 bioanalyzer (Agilent Technologies, Santa Clara, CA), RNAs were sequenced in the HiSeq4000 systems (Illumina, San Diego, CA). Triplicate RNA samples from independent groups were prepared for sequencing. The primary bioinformatic analysis was carried out by Genedenovo Biotechnology (Guangzhou, China). Deseq2 algorithm was used for differential gene analysis, and $|\log2 \text{ fold change}| \geq 1$ and FDR < 0.05 were used as the screening criteria.

In order to examine the correlation between the expression level of *NR0B1* and that of *NRF2*, *c-JUN* and *CBS* in the tumor tissues of lung cancer patients, we also downloaded the relevant gene expression profiles of lung adenocarcinoma (n = 677) and lung squamous cell carcinoma (n = 495) from the cBioPortal for Cancer Genomics Database (v5.3.5). Correlation analysis of the genes expression was performed using Spearman's methods.

Quantitative real-time PCR analysis

Isolated total RNA was reversely transcribed into cDNA using the RevertAid First Strand cDNA Synthesis Kit (Thermofisher Scientific, Waltham, MA). RT-PCR was performed using

2×SYBR Green qPCR Master Mix (Selleck) and detected by the CFX96 real-time PCR detection system (Bio-Rad, Hercules, CA). GAPDH was used as an internal reference. The relative expression levels were normalized using the ΔΔCt method. The primers used in RT-PCR are listed in Table S3.

Western blot analysis

Cells were washed three times with PBS, collected, and lysed with RIPA lysis buffer, including the phosphatase inhibitor cocktail 3 (MCE, HY-K0010). Protein concentrations were determined using the Pierce™ BCA Protein Assay Kit (Thermofisher Scientific). Equal amounts of proteins were loaded into SDS-PAGE and were detected using corresponding antibodies. Information regarding the antibodies used in this experiment is listed in Table S4.

Dual-luciferase reporter assay

Constructed luciferase reporter vectors were transfected into the NR0B1-KD A549 cells, NR0B1-OE H1299 cells, and their respective control cells. After the cells were lysed, luciferase activity in each cell lysate was measured using a dual-luciferase reporter assay system (Promega) following the manufacturer's instructions. Renilla luciferase activity was used as an internal control.

ChIP-qPCR assay

The ChIP assay was executed using the Tag-ChIP-IT kit (Active Motif, Carlsbad, CA). Briefly, cells cultured to 70-80% confluence were harvested and fixed with 1% freshly prepared formaldehyde. The fixed chromatin was sonicated into fragments ranging from 200 to 1000 bp and then immunoprecipitated using corresponding antibodies. The precipitated DNA was subsequently amplified using specific qPCR primers (Table S5).

Co-immunoprecipitation (Co-IP)

Considering that c-JUN and NRF2 naturally associate into heterogeneous oligomers [32], we examined the interaction between c-JUN and NRF2 proteins through Co-IP methods. Briefly, cell lysates were first incubated with anti-c-JUN, anti-NRF2, or IgG. Subsequently, the immune complex was enriched and separated with protein A/G magnetic beads. Finally, the Co-IP proteins were detected by Western blotting with anti-c-JUN or anti-NRF2 antibodies.

Mouse xenograft model

Eight-week-old BALB/c male nude mice were purchased from GemPharmatech (Nanjing) and bred under specific-pathogen-free (SPF) conditions in the Laboratory Animal Center, West China Hospital, Sichuan University. All animal studies were conducted in accordance with the National Research Council's Guide for the Care and Use of Laboratory Animals (USA) and were approved by the Experimental Animal Ethics Committee of West China Hospital in Sichuan University (No.: 2019-772).

Nude mice were divided into two groups (n = 5 per group, randomly). 1×10^6 NR0B1-KD cells of A549 and H1437 were subcutaneously injected into the left armpit of each mouse, respectively, while the same number of wild-type cells from A549 and H1437 were injected into the right armpit of each mouse. Tumor size and body weight were measured twice a week, and tumor volumes were calculated as follows: Volume (mm^3) = (length × $width^2$)/2. To investigate the in vivo effect of RSL3, once the tumor volume reached 200 mm^3, mice were treated with 10 mg/kg RSL3 intratumorally every two or three days for three weeks. After euthanization, tumors were dissected, and the internal MDA and iron levels were measured.

Statistical analysis

All experiments were completed with at least three replicates, presented as mean ± SD. The means of two groups were compared using unpaired Student's t-tests. One-way analysis of variance (ANOVA) was used for comparisons among different groups. All data were analyzed by SPSS 19.0 (IBM, New York). A P value < 0.05 was considered statistically significant.

Results

NR0B1 protects against erastin- or RSL3-induced ferroptosis in lung cancer cells

To explore the role of NR0B1 in lung cancer, we initially selected six lung cancer cell lines. Three of these (A549, H1437, and H460) exhibited

constitutive NR0B1 expression, while the other three (H1975, H1299, and H838) did not. Using lentiviral vectors, we established six cell lines that stably overexpressed exogenous NR0B1 and three cell lines that down-regulated NR0B1 expression (Figure S1). To mitigate potential off-target effects, we restored NR0B1 expression in the NR0B1-depleted cells by overexpressing a shRNA-resistant NR0B1 mutant, which contained an 11-nt mismatch to the shNR0B1 sequence (Table S1). NR0B1 expression was verified across all cell lines (Figure S1).

These cell lines were treated with various concentrations of RSL3 ((1S, 3R)-RSL3) to inhibit glutathione peroxidase 4 (GPX4) activity and induce ferroptosis [27]. The data revealed that RSL3 reduced cell viability in a dose-dependent manner. Moreover, NR0B1-overexpression (NR0B1-OE) mitigated this decrease in viability (**Figure 1A-F**), while down-regulating NR0B1 accelerated cell death (**Figure 1A-C**). Restoring NR0B1 expression restricted cell line sensitivity in NR0B1-knockdown (NR0B1-KD) cells (**Figure 1A-C**). When treating the cells with another commonly used ferroptosis inducer erastin, which inhibits the system X_c^- activity of cystine import [3], NR0B1 also protected against erastin-induced cell death (**Figure 1G-L**). We selected RSL3 to induce ferroptosis in subsequent investigations.

To further confirm NR0B1's involvement in ferroptosis, we measured the intracellular levels of iron, ROS, GSH, and MDA (an end product of lipid peroxidation) in lung cancer cells treated with RSL-3. As anticipated, NR0B1-OE decreased intracellular levels of iron, MDA, and ROS, and increased intracellular GSH levels (**Figure 2A-M**). Conversely, NR0B1-knockdown (NR0B1-KD) increased levels of iron, MDA, and ROS, and decreased GSH levels (**Figure 2A-C**, **2E-G**, **2I-K**, **2M**). Additionally, rescuing the expression of NR0B1 in NR0B1-KD cells increased GSH levels and reduced iron, MDA, and ROS levels (**Figure 2A-C**, **2E-G**, **2I-K**, **2M**). Collectively, these results indicate that NR0B1 suppresses ferroptosis by regulating intracellular levels of iron, MDA, ROS, and GSH.

NR0B1 regulates the expression of ferroptosis-related genes

Erastin and RSL3 have been reported to target system X_c^- and GPX4 respectively. We investigated the expression levels of system X_c^- and GPX4 in lung cancer cells with either overexpressed or down-regulated NR0B1. Results did not demonstrate an evident effect of NR0B1 on the protein levels of system X_c^- and GPX4 (Figure S2), suggesting alternative mechanisms driving NR0B1-suppression of ferroptosis in these cells.

Considering NR0B1 acts as a transcriptional factor, we performed RNA-seq in NR0B1-overexpressed and -knockdown A549 cells (Raw sequence data were submitted to GEO Profiles under accession number: GSE226285). We identified that 375 genes were up-regulated and 200 genes were down-regulated in NR0B1-OE cells (FDR < 0.05, |log2 (fold change)| ≥ 1, Table S6), and 281 genes were up-regulated and 228 genes were down-regulated in NR0B1-KD cells (FDR < 0.05, |log2 (fold change)| ≥ 1, Table S7). Among 478 genes involved in ferroptosis (FerrDb V2, http://www.zhounan.org/ferrdb/current/), twelves were found to be differently expressed in NR0B1-KD or/and NR0B1-OE cells (**Figure 3A-D**; Tables S8, S9). Among them, *ATF3*, *GOT1*, *c-JUN* and *CBS* regulate cysteine metabolism and thereby affect GSH metabolism [33-36]; *NRF2* affects ROS levels by regulating antioxidant gene expression [31]; *NCOA4*, *HSPB1* and *HMOX1* are involved in the regulation of intracellular iron levels [37-39]; *SAT1* regulates lipid metabolism by controlling lipid peroxidation levels [40]; *SLC38A1* enhances L-glutamine absorption, thus affecting glutamine metabolism [41]; and *AKR1C2* [42] and *CS* [43] are involved in lipid peroxidation and lipid metabolism, respectively. Collectively, the differential expression of these genes suggests that NR0B1 inhibits ferroptosis by regulating intracellular levels of iron, lipid peroxidation and GSH.

The different expression of *c-JUN* was observed in both NR0B1-OE and NR0B1-KD cells. c-JUN, the first identified oncogenic transcription factor [44], has been found to transcriptionally upregulate CBS expression, leading to GSH increase and ferroptosis reduction in liver cancer [35]. Additionally, NRF2 also transcriptionally promotes CBS expression to resist ferroptosis in ovarian cancer cells [45]. Here, *c-JUN*, *NRF2*, and *CBS* expression was observed to be significantly decreased in the NR0B1-KD cells (**Figure 3B**, **3D**). Moreover, we extracted RNA-seq data from lung cancer patients (n = 1,172) in the

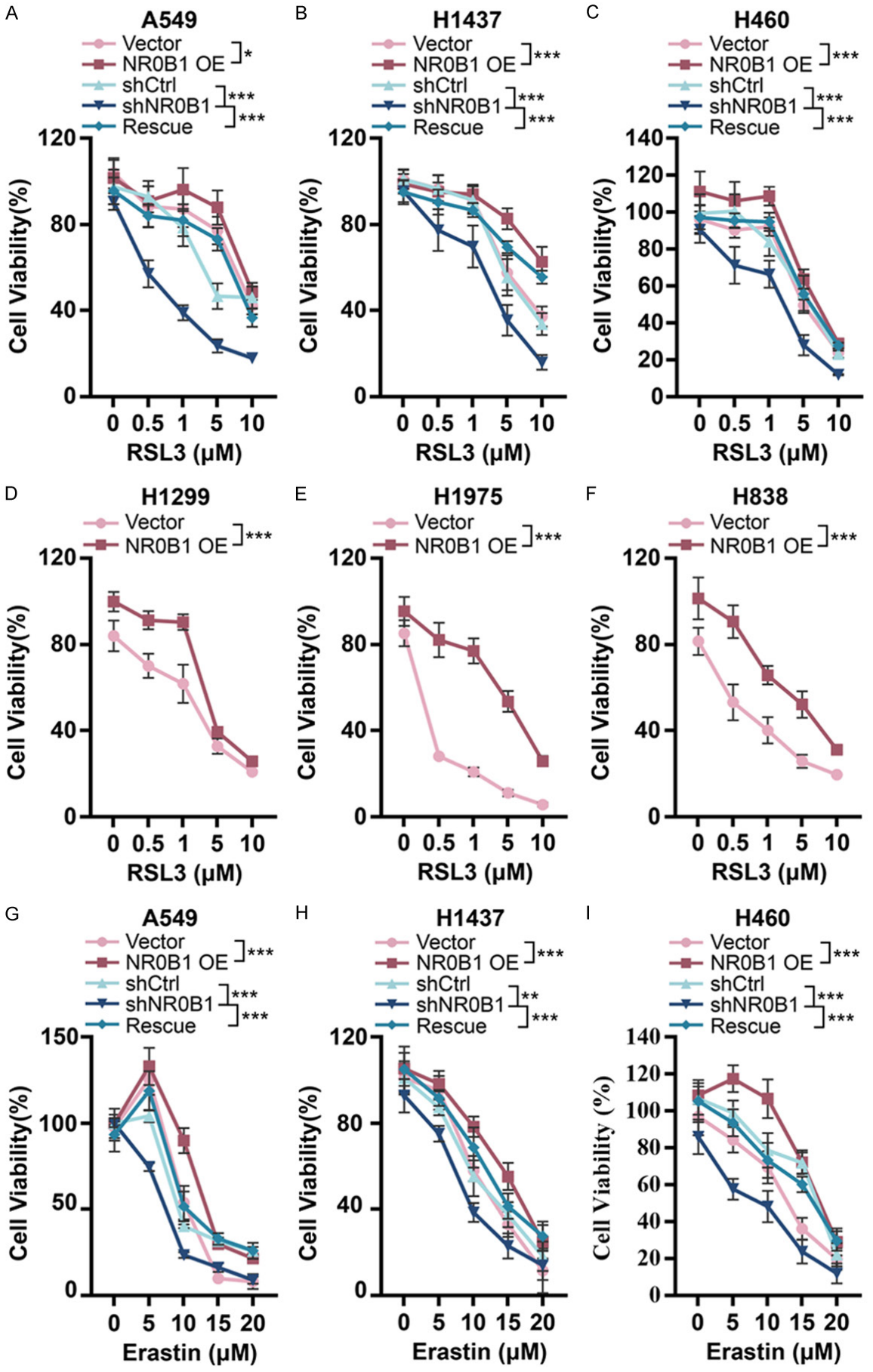
A
A549
Vector
NR0B1 OE
shCtrl
shNR0B1
Rescue
*
***
***
Cell Viability(%)
RSL3 (μM)
B
H1437
***
***
***
C
H460
***
***
***
D
H1299
***
E
H1975
***
F
H838
***
G
A549
***
***
***
H
H1437
***
**
***
I
H460
***
***
***
Erastin (μM)

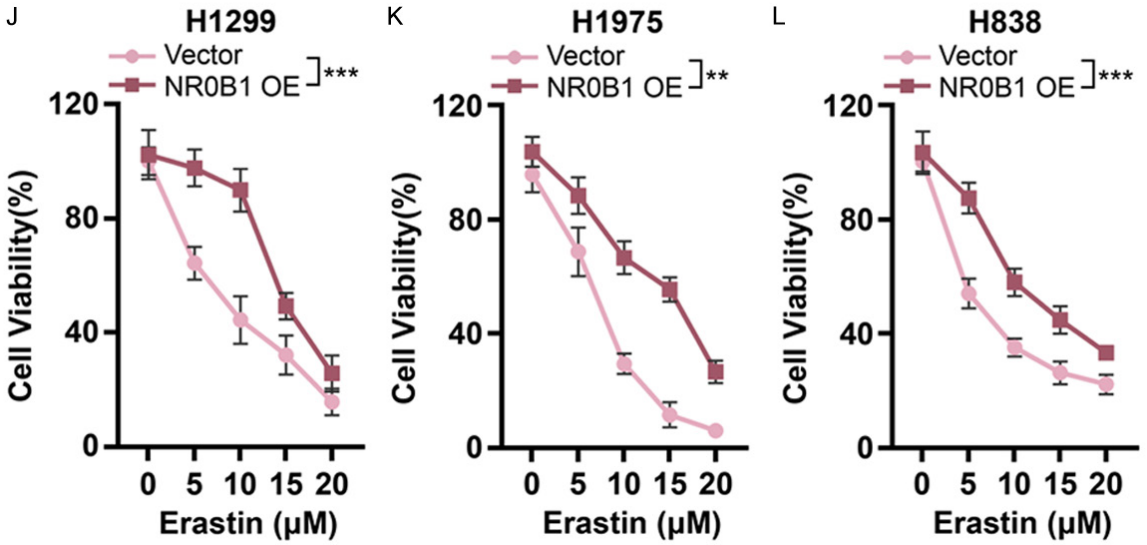

Figure 1. NR0B1 protects against RSL3- or erastin-induced cell death in lung cancer cells. (A-F) Cell viabilities of different lung cancer cells including A549 (A), H1437 (B), H460 (C), H1299 (D), H1975 (E) and H838 (F) under the treatment with different concentrations of RSL3 (0, 0.5, 1, 5, 10 μM). (G-L) Cell viabilities of different lung cancer cells including A549 (G), H1437 (H), H460 (I), H1299 (J), H1975 (K) and H838 (L) under the treatment with different concentrations of erastin (0, 5, 10, 15, 20 μM). Vector: overexpression vehicle control, NR0B1 OE: NR0B1-overexpression, shCtrl: knockdown vehicle control, shNR0B1: NR0B1-knockdown, shNR0B1-res: rescued NR0B1-expression after NR0B1-knockdown. Data are presented as mean ± SD, n = 3, $*P < 0.05$, $**P < 0.01$, $***P < 0.001$.

cBioPortal for Cancer Genomics Database (http://cbioportal.org) to explore the correlation between the expression levels of *NR0B1* and *c-JUN*, *NRF2* and *CBS*. We found that the *NR0B1* expression was activated in the tumors from more than half of the patients (Figure S3A, RNA-Seq by Expectation-Maximization (RSEM) > 0). In these NR0B1-activated lung tumors, we observed that the expression level of *NR0B1* was positively correlated with that of *NRF2* (**Figure 3E**), *c-JUN* (**Figure 3F**) and *CBS* (**Figure 3G**) separately, and similarly, the expression level of *CBS* was also correlated with *NRF2* (Figure S3B) and *c-JUN* (Figure S3C), supporting that NRF2 and c-JUN promote *CBS* transcription. Thus, we proposed that the four genes of *NR0B1*, *c-JUN*, *NRF2* and *CBS* may be involved in a cross-talk network in lung cancer cells (**Figure 3H**), although the mechanisms involved need to be further elucidated. Furthermore, it was confirmed that the expression of *c-JUN*, *NRF2* and *CBS* was regulated by NR0B1 (**Figure 3I-O**). Therefore, the three genes of *c-JUN*, *NRF2,* and *CBS* were included in further investigations into the mechanism by which NR0B1 antagonizes ferroptosis.

NR0B1-mediated ferroptosis resistance depends on the activities of c-JUN, NRF2 and CBS

To further investigate the role of NRF2, c-JUN and CBS in NR0B1-driven inhibition of ferroptosis, we evaluated the effect of NRF2 and c-JUN on NR0B1-mediated resistance to RSL3-induced ferroptosis. First, we treated NRF2 or c-JUN knockdown lung cancer cells with varying concentrations of RSL3 and observed that down-regulation of NRF2 or c-JUN accelerated cell death, increased the intracellular levels of iron, MDA, and ROS, and reduced intracellular GSH levels (Figures S4 and S5). These findings suggest that both NRF2 and c-JUN contribute to the suppression of ferroptosis in lung cancer cells. In NR0B1-KD cells, we discovered that overexpression of *NRF2* or *c-JUN* increased cell survival (**Figure 4A**, **4B**) and decreased the intracellular iron (**Figure 4C**, **4D**) and MDA levels (**Figure 4E**, **4F**). In NR0B1-OE cells, knockdown of *NRF2* or *c-JUN* enhanced RSL3-induced cell death (**Figure 4G**, **4H**) and elevated intracellular iron (**Figure 4I**, **4J**) and MDA levels (**Figure 4K**, **4L**). These results suggest that the ferroptosis-resistance mediated by NR0B1 is

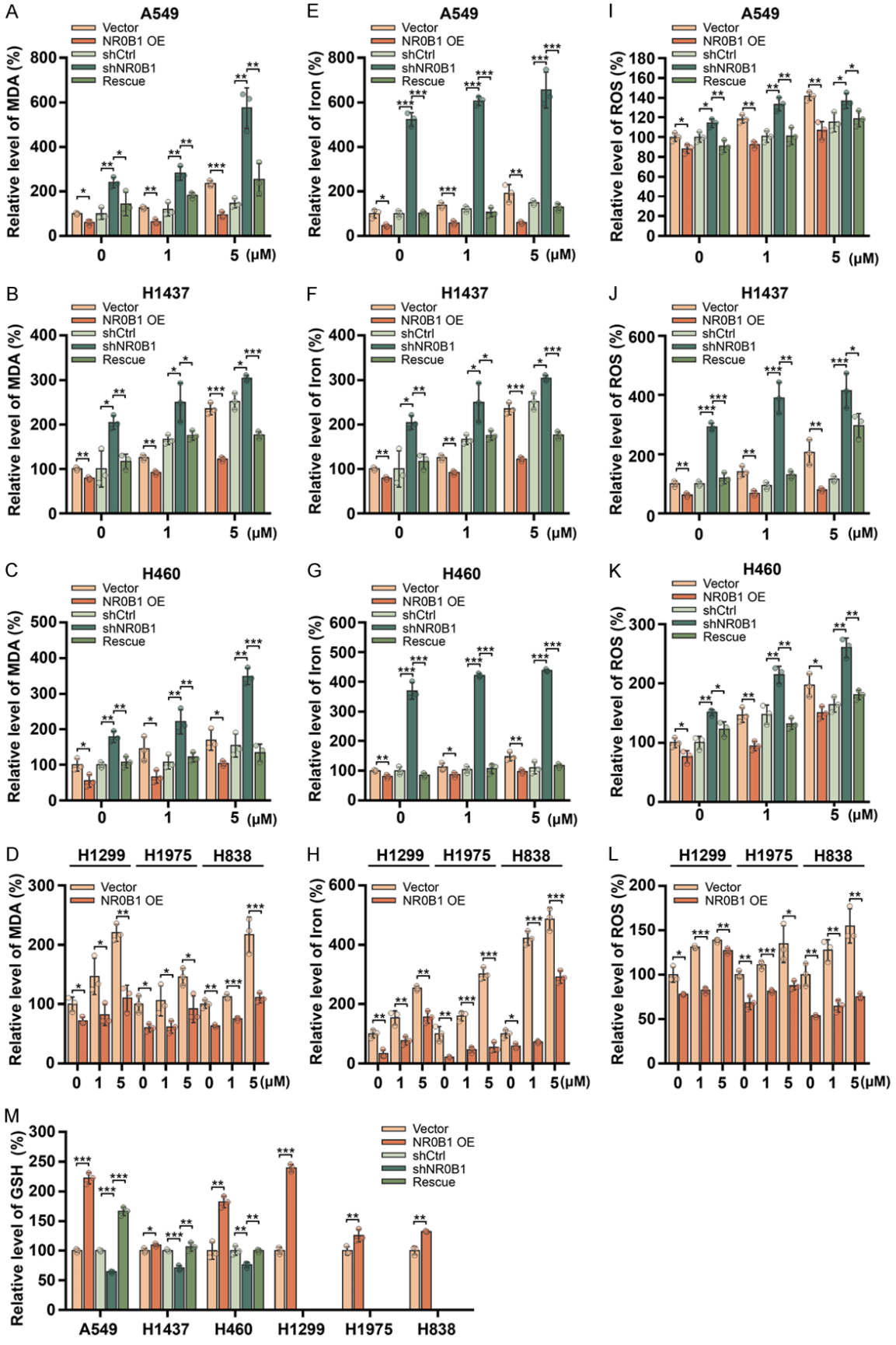
A
A549
Vector
NR0B1 OE
shCtrl
shNR0B1
Rescue
Relative level of MDA (%)
0
200
400
600
800
0
1
5 (μM)
E
A549
Relative level of Iron (%)
I
A549
Relative level of ROS (%)
B
H1437
Relative level of MDA (%)
F
H1437
Relative level of Iron (%)
J
H1437
Relative level of ROS (%)
C
H460
Relative level of MDA (%)
G
H460
Relative level of Iron (%)
K
H460
Relative level of ROS (%)
D
H1299
H1975
H838
Relative level of MDA (%)
0 1 5 0 1 5 0 1 5(μM)
H
H1299
H1975
H838
Relative level of Iron (%)
L
H1299
H1975
H838
Relative level of ROS (%)
M
Relative level of GSH (%)
A549
H1437
H460
H1299
H1975
H838

Figure 2. NR0B1 restrains RSL3 induced ferroptosis in lung cancer cells. (A-D) Relative MDA levels in the lung cancer cells of A549 (A), H1437 (B), H460 (C), H1299 (D), H1975 (D) and H838 (D) under the treatment with different concentrations of RSL3 (0, 1, 5 μM). (E-H) Relative iron levels in the cells of A549 (E), H1437 (F), H460 (G), H1299 (H), H1975 (H) and H838 (H) treated with RSL3. (I-L) Relative ROS levels in the cells of A549 (I), H1437 (J), H460 (K), H1299 (L), H1975 (L) and H838 (L) treated with RSL3. (M) Relative GSH levels in the lung cancer cells treated with RSL3. Data are presented as mean ± SD, n = 3, **P* < 0.05, ***P* < 0.01, ****P* < 0.001.

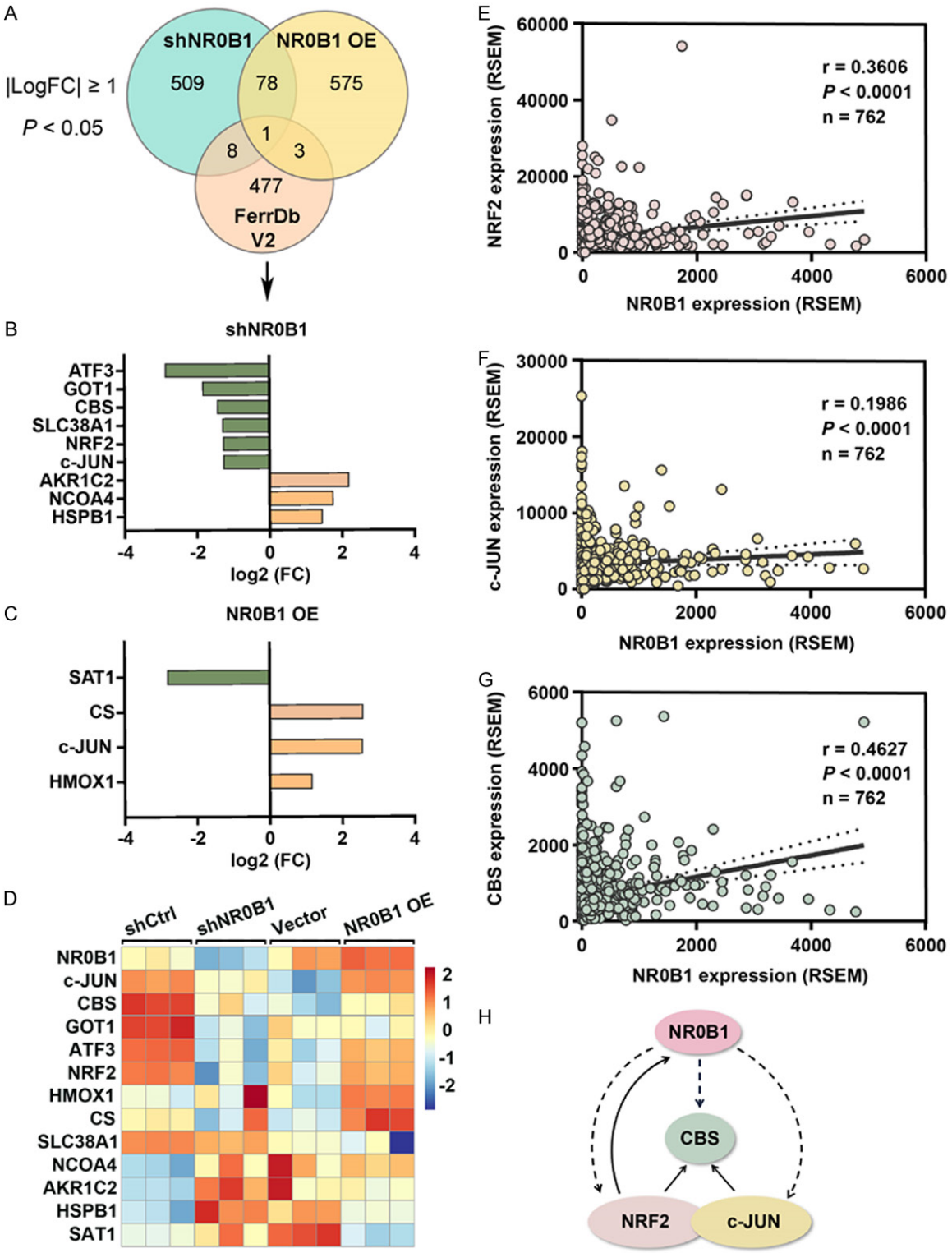

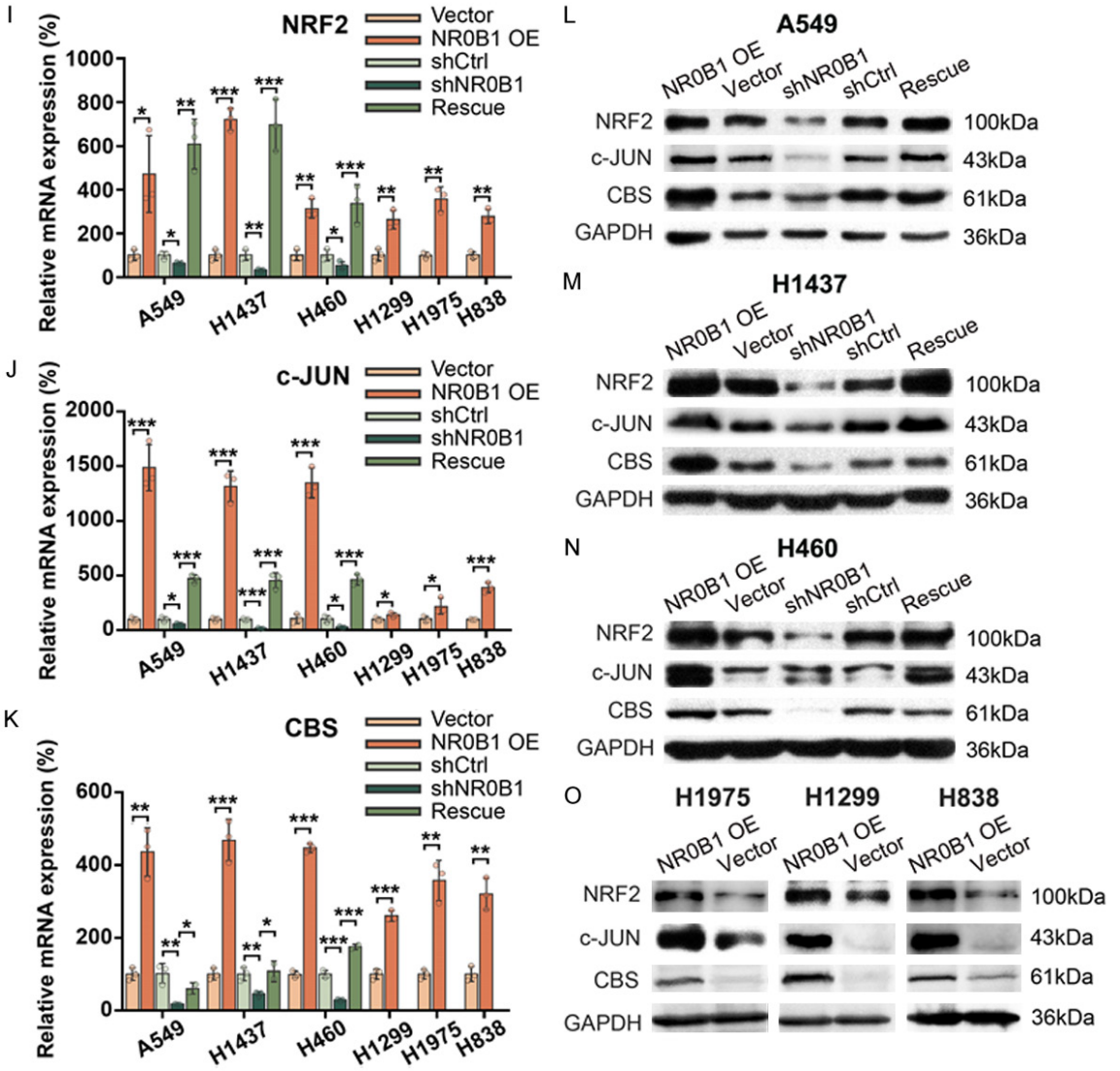

Figure 3. Transcriptomic data reveals the ferroptosis-related genes under the NR0B1 regulation. (A) Venn Diagram showing the numbers of differentially expressed genes (DEGs) obtained by RNA-Seq in NR0B1-OE and -KD A549 cells (FDR < 0.05, |log2 (fold change)| ≥ 1), and that reportedly involved in ferroptosis (FerrDb V2). (B) Nine ferroptosis-related DEGs identified in NR0B1-KD cells. (C) Four ferroptosis-related DEGs identified in NR0B1-OE cells. (D) Heat map showing the different expression of *NR0B1* and the 12 ferroptosis-related DEGs. (E-G) The expression level of three ferroptosis-associated DEGs, including *NRF2* (E), *c-JUN* (F) and *CBS* (G), were positively correlated with the *NR0B1* expression in lung tumors (based on transcriptomic data from the cBioPortal for Cancer Genomics Database). (H) Cross-talk between the four genes of *NR0B1*, *c-JUN*, *NRF2* and *CBS*. Solid arrows show the reported links and dashed arrows indicate the speculated regulatory pathways. (I-K) The expression levels of *NRF2* (I), *c-JUN* (J) and *CBS* (K) were verified by real-time quantitative PCR analysis in different lung cancer cells. Data are presented as mean ± SD, n = 3, **P* < 0.05, ***P* < 0.01, ****P* < 0.001. (L-O) The protein levels of c-JUN, NRF2 and CBS were verified in the cells of A549 (L), H1437 (M), H460 (N), H1299 (O), H1975 (O) and H838 (O) by Western Blot analysis.

associated with the upregulation of the NRF2 and c-JUN.

Subsequently, cells were treated with a CBS inhibitor, AOA hemihydrochloride (AOAA), revealing that AOAA significantly reduced the effect of NR0B1 on cell viability while inhibiting the suppressive effect of NR0B1 on RSL3-induced cell death (**Figure 5A**, **5B**). Additionally, siRNA was used to reduce CBS expression (Figure S6); similar effects were found to that of AOAA on the RSL3-induced cell death (**Figure 5C**, **5D**). Concurrently, we observed that inhibiting CBS activity with AOAA or siRNA in NR0B1-OE cells

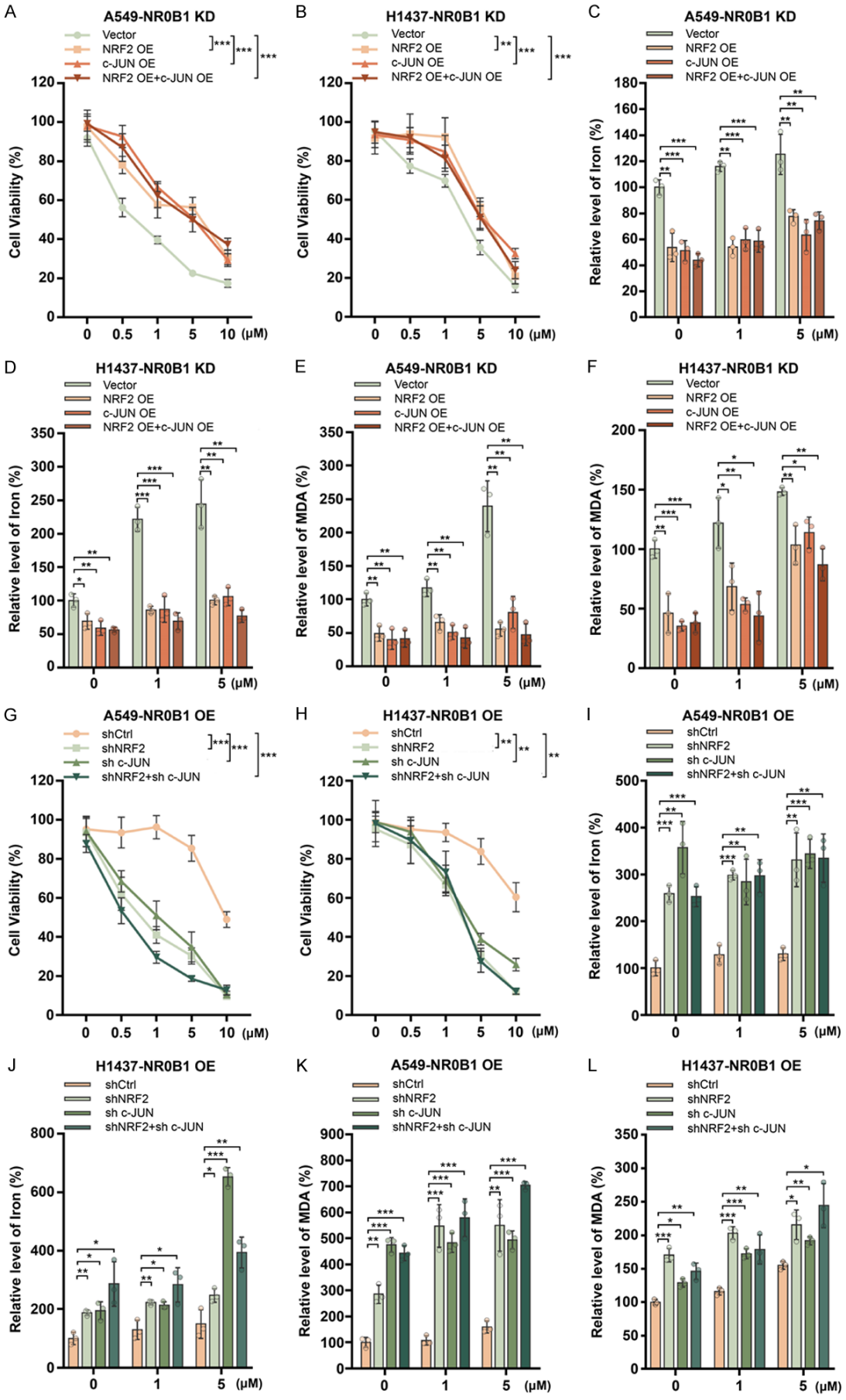
A
A549-NR0B1 KD
Vector
NRF2 OE
c-JUN OE
NRF2 OE+c-JUN OE
Cell Viability (%)
0 0.5 1 5 10 (μM)
B
H1437-NR0B1 KD
C
A549-NR0B1 KD
Relative level of Iron (%)
0 1 5 (μM)
D
H1437-NR0B1 KD
E
A549-NR0B1 KD
Relative level of MDA (%)
F
H1437-NR0B1 KD
G
A549-NR0B1 OE
shCtrl
shNRF2
sh c-JUN
shNRF2+sh c-JUN
H
H1437-NR0B1 OE
I
A549-NR0B1 OE
J
H1437-NR0B1 OE
K
A549-NR0B1 OE
L
H1437-NR0B1 OE

Figure 4. NR0B1 suppressing ferroptosis depends on the activities of c-JUN and NRF2. (A, B) Cell viabilities of NR0B1-KD A549 (A) and H1437 (B) cells under the combined treatments with the overexpression of c-JUN or/and NRF2 and different concentrations of RSL3. (C, D) Relative iron levels in the NR0B1-KD A549 (C) and H1437 (D) cells under the combined treatments with the overexpression of c-JUN or/and NRF2 and different concentrations of RSL3. (E, F) Relative MDA levels in the NR0B1-KD A549 (E) and H1437 (F) cells under the combined treatments with the overexpression of c-JUN or/and NRF2 and different concentrations of RSL3. (G, H) Cell viabilities of NR0B1-OE A549 (G) and H1437 (H) cells under the combined treatments with the downregulation of c-JUN or/and NRF2 and different concentrations of RSL3. (I, J) Relative iron levels in the NR0B1-OE A549 (I) and H1437 (J) cells under the combined treatments with the downregulation of c-JUN or/and NRF2 and different concentrations of RSL3. (K, L) Relative MDA levels in the NR0B1-OE A549 (K) and H1437 (L) cells under the combined treatments with the downregulation of c-JUN or/and NRF2 and different concentrations of RSL3. Vector: overexpression vehicle control, shCtrl: knockdown vehicle control. Data are presented as mean ± SD, n = 3, $*P < 0.05$, $**P < 0.01$, $***P < 0.001$.

distinctly decreased GSH levels (**Figure 5E-H**) and increased iron (**Figure 5I-L**) and MDA levels (**Figure 5M-P**). These findings indicate that inhibiting CBS activity mitigated the suppressive effect of NR0B1 on ferroptosis, suggesting that the NR0B1-driven ferroptosis-resistance also depends on the upregulation of CBS.

NR0B1 directly promotes the expression of NRF2 and c-JUN but not CBS

We next investigated whether NR0B1, functioning as a transcriptional factor, directly promotes *CBS* expression. Through in silico analysis (http://jaspar.genereg.net) using the animal transcription factors database (HumanTFDB V3.0, http://bioinfo.life.hust.edu.cn/AnimalTFDB), we predicted three potential NR0B1-binding elements (NREs) in the CBS promoter region from -2640 bp to +231 bp (**Figure 6A**). After constructing CBS-driven luciferase expression vectors with various promoter length, we observed that the NR0B1 expression upregulated the *CBS* promoter activity (**Figure 6B**, **6C**). However, the chromatin immunoprecipitation (ChIP)-quantitative polymerase chain reaction (qPCR) analysis did not detect NR0B1 binding to the aforementioned three predicted sites in the CBS promoter in two lung cancer cells (**Figure 6D**, **6E**), suggesting that NR0B1 might indirectly enhance CBS transcription.

Given that NRF2 and c-JUN have been reported to transcriptionally upregulate CBS expression [33, 34] and that NR0B1 was found to promote the expression of NRF2 and c-JUN in this study, we hypothesized that NR0B1 may directly influence the transcription of *c-JUN* and *NRF2*, and that the increased expression of these two genes further enhances CBS transcription. To validate this hypothesis, we predicted three potential NREs in the promoter regions of NRF2 (from -2335 bp to +250 bp, **Figure 6F**) and c-JUN (from -2037 bp to +109 bp, **Figure 6G**). Subsequent luciferase activity assays revealed that NR0B1 notably upregulated the promoter activities of NRF2 and c-JUN (**Figure 6H**, **6I**). Moreover, the ChIP-qPCR assay demonstrated that NR0B1 bound to the promoter regions of NRF2 and c-JUN (**Figure 6J**, **6K**), suggesting that NR0B1 directly promotes the transcription of NRF2 and c-JUN.

NR0B1 upregulates the CBS expression through enhancing the transcriptional activity of NRF2 and c-JUN

NRF2 and c-JUN have been reported to form heterodimers that act on target genes containing antioxidant response elements (AREs) in the promoter region [32]. In this context, we confirmed that c-JUN and NRF2 formed a complex in lung cancer cells (**Figure 7A**) and identified three potential ARE sites in the CBS promoter (**Figure 7B**). We observed that overexpression of c-JUN and/or NRF2 distinctly enhanced CBS promoter activity in NR0B1-KD cells (**Figure 7C**), while down-regulating the expression of c-JUN and/or NRF2 decreased CBS promoter activity in NR0B1-OE cells (**Figure 7D**). The ChIP-qPCR assay revealed that both c-JUN and NRF2 bound to one of the three predicted ARE sites in the CBS promoter (**Figure 7E**, **7F**), suggesting that the NRF2 and c-JUN dimer directly regulates CBS promoter activity.

Moreover, we discovered that overexpression of NRF2 and/or c-JUN significantly increased CBS expression at the mRNA and protein levels in NR0B1-KD cells (**Figure 7G-J**), while in NR0B1-OE cells, knockdown of NRF2 and/or c-JUN markedly decreased CBS expression (**Figure 7K-N**). In summary, these findings revealed that NR0B1 promoted CBS expression by upregulating the transcriptional activity of NRF2 and c-JUN.

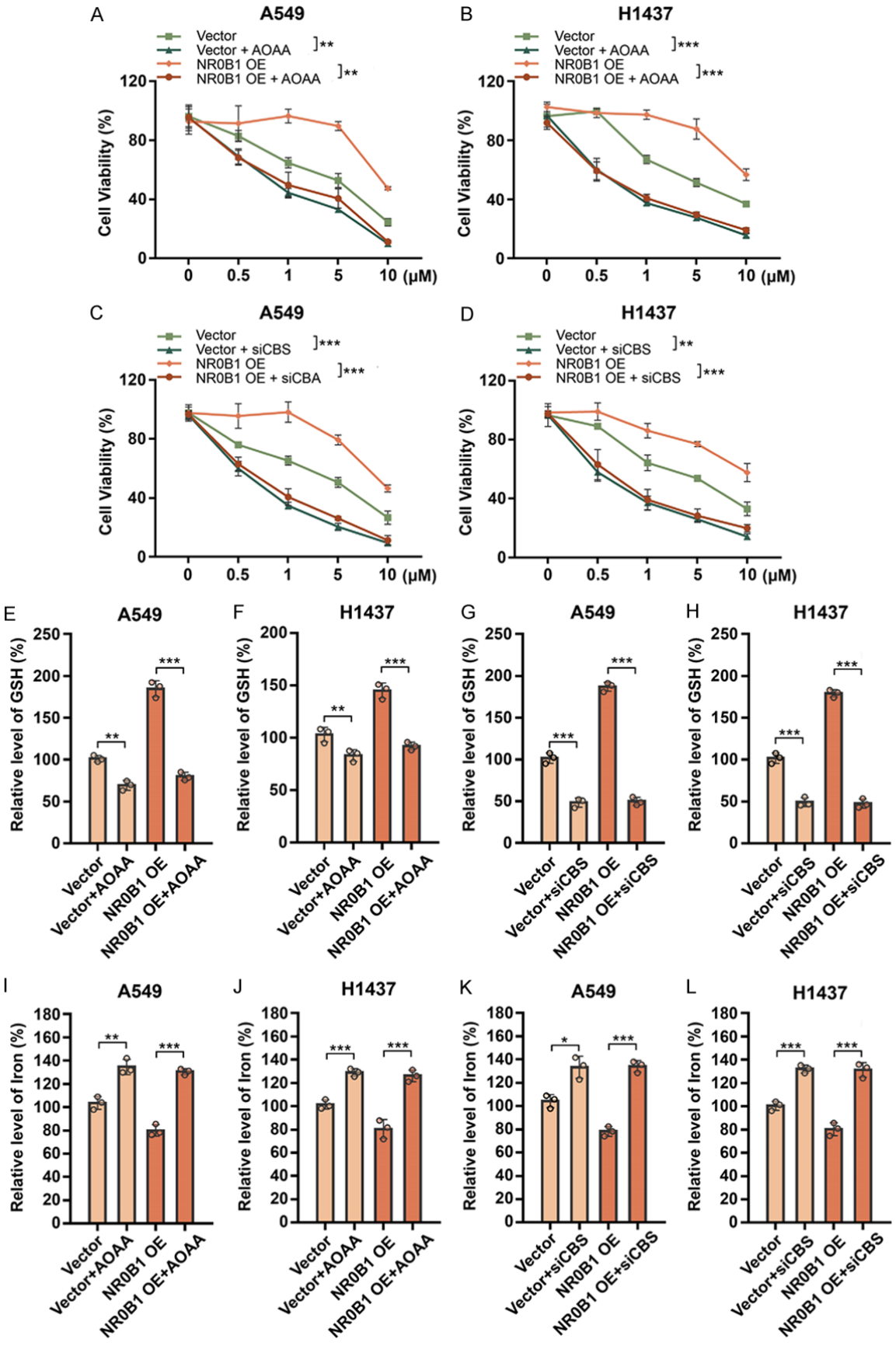
A
A549
Vector
Vector + AOAA
NR0B1 OE
NR0B1 OE + AOAA
]**
]**
Cell Viability (%)
120
80
40
0
0
0.5
1
5
10 (μM)
B
H1437
Vector
Vector + AOAA
NR0B1 OE
NR0B1 OE + AOAA
]***
]***
Cell Viability (%)
C
A549
Vector
Vector + siCBS
NR0B1 OE
NR0B1 OE + siCBA
]***
]***
Cell Viability (%)
D
H1437
Vector
Vector + siCBS
NR0B1 OE
NR0B1 OE + siCBS
]**
]***
Cell Viability (%)
E
A549
Relative level of GSH (%)
250
200
150
100
50
0
**
***
Vector
Vector+AOAA
NR0B1 OE
NR0B1 OE+AOAA
F
H1437
Relative level of GSH (%)
200
150
100
50
0
**
***
Vector
Vector+AOAA
NR0B1 OE
NR0B1 OE+AOAA
G
A549
Relative level of GSH (%)
250
200
150
100
50
0
***
***
Vector
Vector+siCBS
NR0B1 OE
NR0B1 OE+siCBS
H
H1437
Relative level of GSH (%)
250
200
150
100
50
0
***
***
Vector
Vector+siCBS
NR0B1 OE
NR0B1 OE+siCBS
I
A549
Relative level of Iron (%)
180
160
140
120
100
80
60
40
20
0
**
***
Vector
Vector+AOAA
NR0B1 OE
NR0B1 OE+AOAA
J
H1437
Relative level of Iron (%)
180
160
140
120
100
80
60
40
20
0
***
***
Vector
Vector+AOAA
NR0B1 OE
NR0B1 OE+AOAA
K
A549
Relative level of Iron (%)
180
160
140
120
100
80
60
40
20
0
*
***
Vector
Vector+siCBS
NR0B1 OE
NR0B1 OE+siCBS
L
H1437
Relative level of Iron (%)
180
160
140
120
100
80
60
40
20
0
***
***
Vector
Vector+siCBS
NR0B1 OE
NR0B1 OE+siCBS

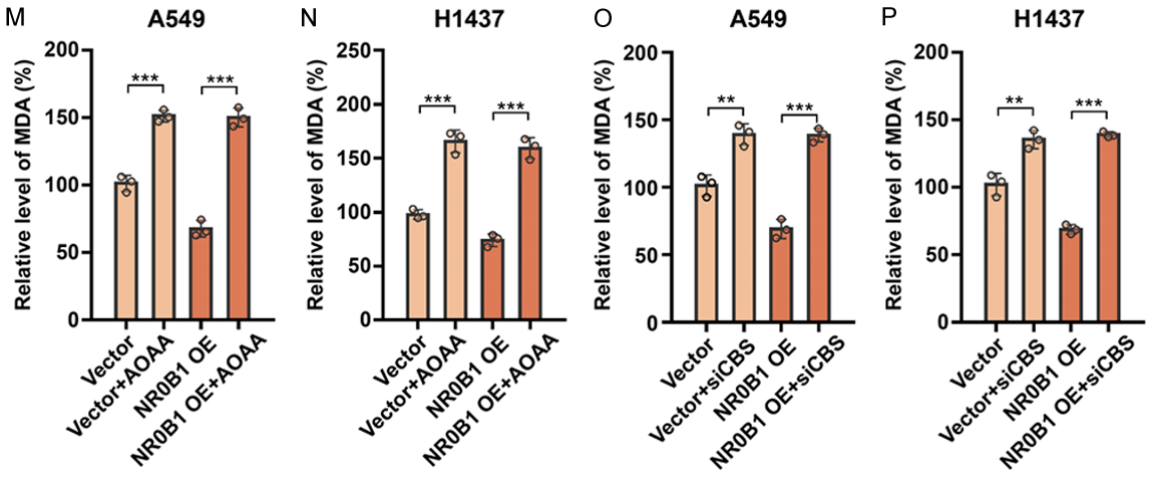

Figure 5. NR0B1 suppressing ferroptosis depends on the CBS activity. (A, B) The effects of CBS inhibitor AOAA on the cell viabilities of NR0B1-OE A549 (A) and H1437 (B) cells under the treatments with RSL3. (C, D) The effects of CBS-KD with siCBS on the cell viabilities of NR0B1-OE A549 (C) and H1437 (D) cells under the treatments with RSL3. (E, F) Relative GSH levels in the NR0B1-OE A549 (E) and H1437 (F) cells treated with RSL3 and AOAA. (G, H) Relative GSH levels in the NR0B1-OE A549 (G) and H1437 (H) cells treated with RSL3 and siCBS. (I, J) Relative iron levels in the NR0B1-OE A549 (I) and H1437 (J) cells treated with RSL3 and AOAA. (K, L) Relative iron levels in the NR0B1-OE A549 (K) and H1437 (L) cells treated with RSL3 and siCBS. (M, N) Relative MDA levels in the NR0B1-OE A549 (M) and H1437 (N) cells treated with RSL3 and AOAA. (O, P) Relative MDA levels in the NR0B1-OE A549 (O) and H1437 (P) cells treated with RSL3 and siCBS. Vector: overexpression vehicle control. Data are presented as mean ± SD, n = 3, $*P < 0.05$, $**P < 0.01$, $***P < 0.001$.

NR0B1-KD restrains the tumor growth and facilitates RSL3-induced ferroptosis

To further explore the effect of NR0B1 on in vivo tumor growth, we subcutaneously implanted NR0B1-KD lung cancer cells into nude mice. We observed that NR0B1-KD significantly inhibited tumor growth of lung cancer cells (**Figure 8A**, **8B**), and the size and weight of xenografts were notably reduced in NR0B1-KD lung cancer cells (**Figure 8C-F**). Additionally, when the xenografts reached approximately 200 mm^3, we treated the tumor-bearing mice with RSL3 and notably observed that RSL3 treatment more effectively restrained tumor growth in mice implanted with NR0B1-KD lung cells juxtaposed to the control group implanted with wild type NR0B1-expressing cells (**Figure 8G**, **8H**). This finding was further substantiated by the examination of xenograft size and weight (**Figure 8I-L**). Moreover, we found that levels of MDA and iron were significantly increased in the NR0B1-KD xenograft compared to the control (**Figure 8M-P**). These results suggest that NR0B1 depletion restrains tumor growth and facilitates RSL3-induced ferroptosis *in vivo*.

Furthermore, we examined the expression levels of NR0B1, NRF2, c-JUN and CBS in the xenografts. Consistent with the outcomes of the *in vitro* experiments, we found that the expression of NRF2, c-JUN and CBS was markedly decreased in the xenografts formed by the NR0B1-KD lung cancer cells (**Figure 8Q**). In summary, our findings revealed that NR0B1 promoted the *in vivo* tumor formation of lung cancer cells and resisted ferroptosis through upregulating the NRF2/c-JUN-CBS signaling activity (**Figure 8R**).

Discussion

Ferroptosis can typically be induced by inhibiting cysteine uptake or by inactivating the lipid repair enzyme GPX4. In lung cancer cells, our current study demonstrated that NR0B1 suppressed ferroptosis. We observed that NR0B1 regulated the transcriptional levels of 12 ferroptosis-related genes. This study primarily focused on the signaling pathway involving the molecules NRF2, c-JUN, and CBS, revealing that NR0B1 directly promoted the transcription of *NRF2* and *c-JUN*. Furthermore, the upregulation of NRF2 and c-JUN subsequently enhanced CBS expression, bolstering ferroptosis resistance. For the first time, this study revealed that the ferroptosis-suppressing capability of

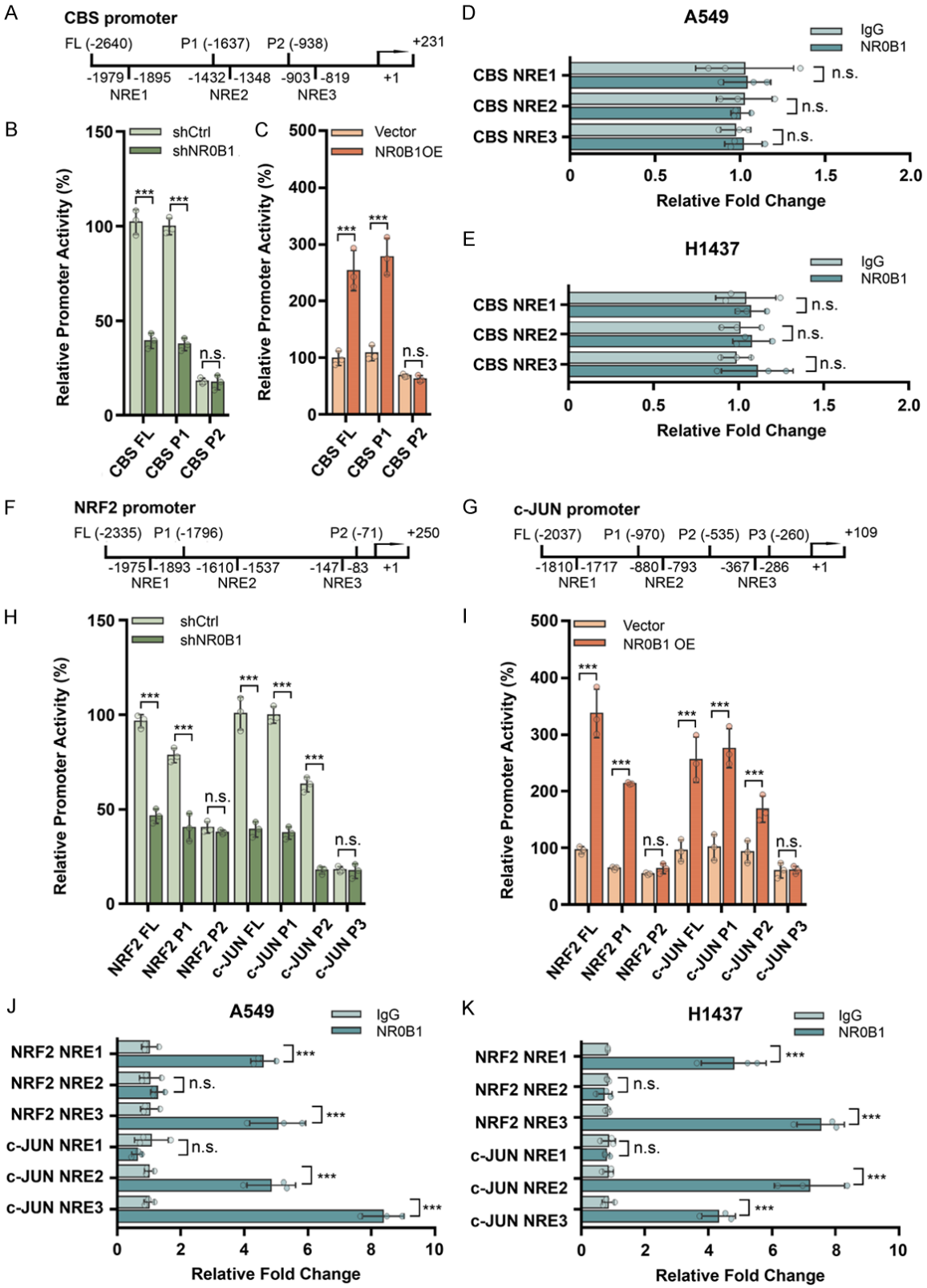

Figure 6. NR0B1 directly promotes the transcription of NRF2 and c-JUN but not CBS. (A) Schematic of the CBS promoter depicting the location of promoter constructs (full length (FL), P1 and P2) and that of predicted NR0B1 binding elements (NRE). (B, C) Luciferase reporter assays showed that the luciferase activity of *CBS* promoter constructs

(FL and P1) were decreased in NR0B1-KD (B) and increased in NR0B1-OE cells (C). (D, E) ChIP-PCR assays showed that the predicted NREs in the *CBS* promoter were not detected in the cells of A549 (D) and H1437 (E). (F, G) Schematic of the NRF2 (F) and c-JUN (G) promoters depicting the location of promoter constructs (FL, P1, P2 and P3) and that of predicted NR0B1 binding elements (NRE). (H, I) Luciferase reporter assays showed that the promoter luciferase activity of *NRF2* (FL and P1) and c-JUN (FL, P1 and P2) were decreased in NR0B1-KD (H) and increased in NR0B1-OE cells (I). (J, K) ChIP-PCR assays showed that the predicted NREs in the promoters of *NRF2* (NRE1 and NRE3) and *c-JUN* (NRE2 and NRE3) were verified in the cells of A549 (J) and H1437 (K). Data are presented as mean ± SD, n = 3, $*P < 0.05$, $**P < 0.01$, $***P < 0.001$. n.s. means no significant difference.

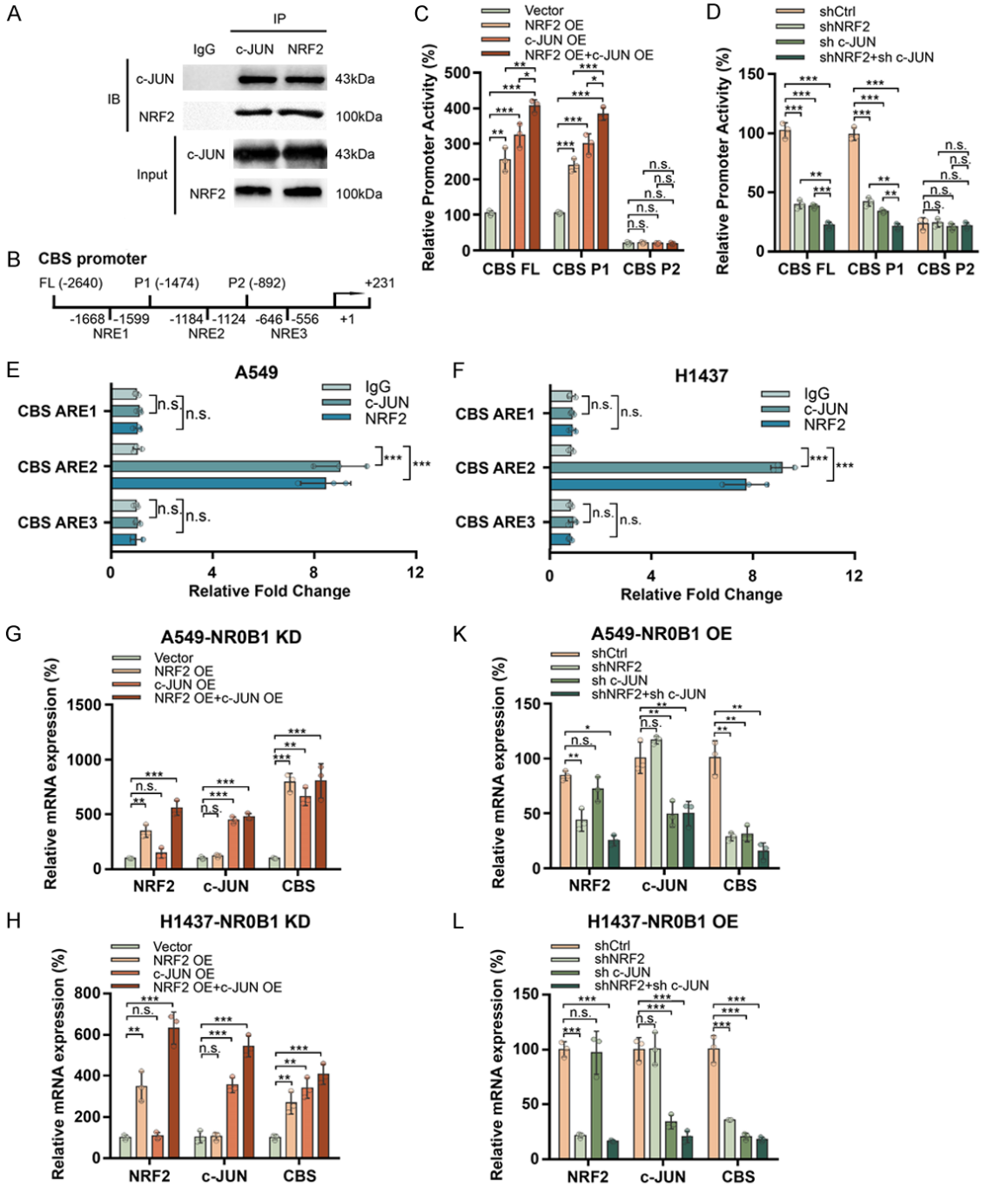

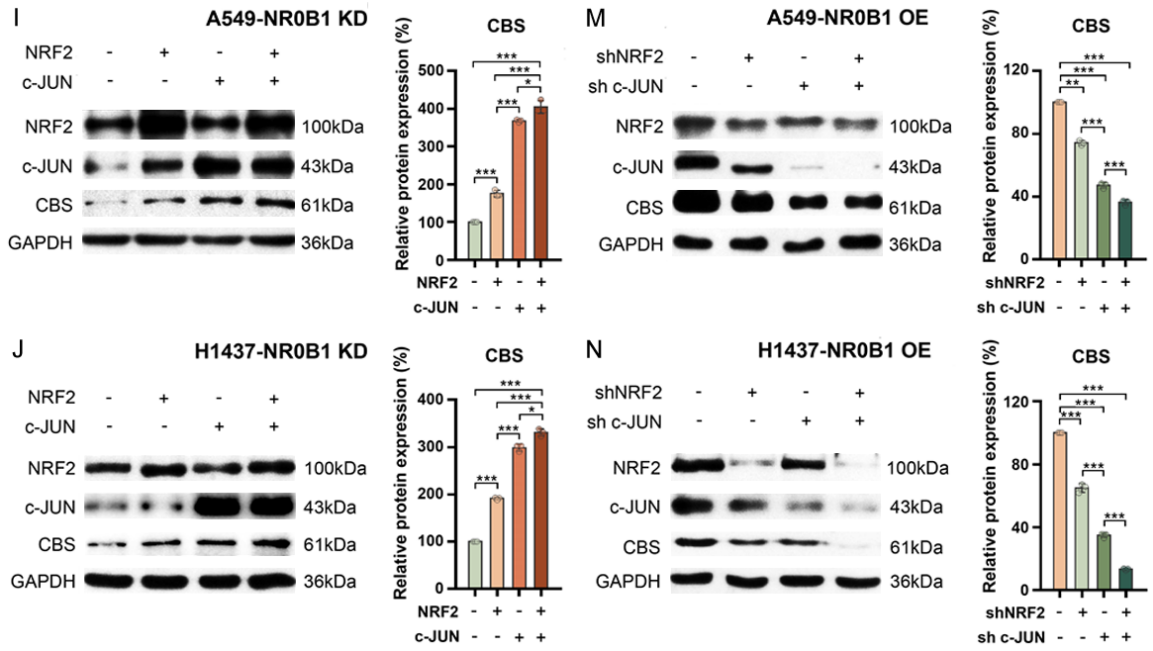

Figure 7. NR0B1 upregulates the CBS expression via the enhancement of the NRF2 and c-JUN activities. (A) The complex of NRF2 and c-JUN was verified in A549 cells by Co-IP assay. (B) Schematic of the *CBS* promoter depicting the predicted antioxidant response elements (AREs) in the *CBS* promoter. (C) Luciferase reporter assays showed that the luciferase activity of *CBS* promoter constructs (FL and P1) were increased in NR0B1-KD A549 cells with the overexpression of c-JUN or/and NRF2. (D) Luciferase reporter assays showed that the luciferase activity of *CBS* promoter constructs (FL and P1) were decreased in NR0B1-OE A549 cells with the downregulation of c-JUN or/and NRF2 (shNRF2, sh c-JUN). (E, F) ChIP-PCR assays showed that one predicted ARE site in the *CBS* promoter (ARE2) was verified in the cells of A549 (E) and H1437 (F). (G, H) The mRNA levels of *CBS* were increased in NR0B1-KD A549 (G) and H1437 (H) cells with the overexpression of c-JUN or/and NRF2. (I, J) The CBS protein levels were increased in NR0B1-KD A549 (I) and H1437 (J) cells with the overexpression of c-JUN or/and NRF2. (K, L) The mRNA levels of *CBS* were decreased in NR0B1-OE A549 (K) and H1437 (L) cells with the downregulation of c-JUN or/and NRF2. (M, N) The CBS protein levels were decreased in NR0B1-OE A549 (M) and H1437 (N) cells with the downregulation of c-JUN or/and NRF2. Vector: overexpression vehicle control, shCtrl: knockdown vehicle control. Data are presented as mean ± SD, n = 3, $*P < 0.05$, $**P < 0.01$, $***P < 0.001$. n.s. means no significant difference.

NR0B1 hinges on the NRF2/c-JUN-CBS pathway axis (**Figure 8R**).

Despite recent advancements, malignant tumors remain challenging to cure, with susceptibility to multidrug resistance (MDR) being a key obstacle [46]. Interestingly, drug-resistant cancer cells, particularly those in a mesenchymal state and prone to metastasis, have been reported to be highly susceptible to ferroptosis [47], indicating that ferroptosis may play a role in the drug responses during cancer therapy. Both RSL3 and erastin have demonstrated an enhancement of the antitumor effects of antitumor drugs, such as temozolomide [48, 49], cisplatin [50, 51] and vemurafenib [52, 53]. Additionally, some ferroptosis inducers, including salazosulfapyridine [54], sorafenib (SRF) [55] and artemisinin [56] are also heralded for their considerable clinical value in tumor treatment. Nonetheless, ferroptosis inducers may activate a negative feedback loop that inhibits ferroptosis [45]. In this study, we found that RSL3 treatment increased the expression of NR0B1, c-JUN, NRF2, and CBS, along with ferroptosis (Figure S7), suggesting that the stress from ferroptosis inducers, similar to some other anti-cancer chemicals [57], may trigger epigenetic reprogramming in cancer cells. Therefore, further investigation into mechanism of how ferroptosis inducers activate ferroptosis suppressors is necessary for developing ferroptosis-based therapies.

Several nuclear receptor families that regulate drug metabolism and transport are gaining recognition for their potential to overcome MDR in malignancies [58]. Most nuclear receptor-tar-

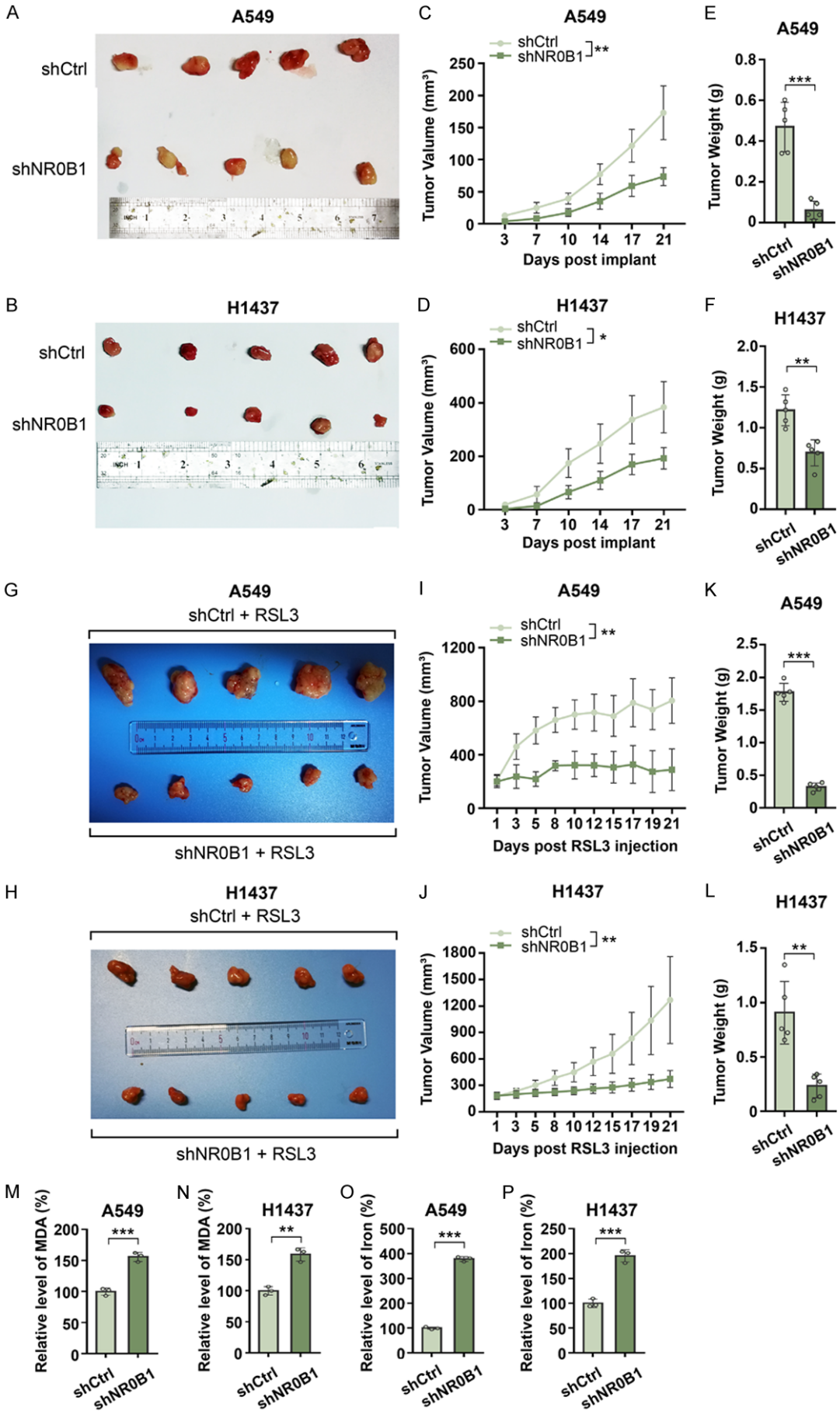
A
A549
shCtrl
shNR0B1
B
H1437
shCtrl
shNR0B1
C
A549
shCtrl
shNR0B1
**
Tumor Valume (mm³)
Days post implant
D
H1437
shCtrl
shNR0B1
*
Tumor Valume (mm³)
Days post implant
E
A549
***
Tumor Weight (g)
shCtrl
shNR0B1
F
H1437
**
Tumor Weight (g)
shCtrl
shNR0B1
G
A549
shCtrl + RSL3
shNR0B1 + RSL3
H
H1437
shCtrl + RSL3
shNR0B1 + RSL3
I
A549
shCtrl
shNR0B1
**
Tumor Valume (mm³)
Days post RSL3 injection
J
H1437
shCtrl
shNR0B1
**
Tumor Valume (mm³)
Days post RSL3 injection
K
A549
***
Tumor Weight (g)
shCtrl
shNR0B1
L
H1437
**
Tumor Weight (g)
shCtrl
shNR0B1
M
A549
***
Relative level of MDA (%)
shCtrl
shNR0B1
N
H1437
**
Relative level of MDA (%)
shCtrl
shNR0B1
O
A549
***
Relative level of Iron (%)
shCtrl
shNR0B1
P
H1437
***
Relative level of Iron (%)
shCtrl
shNR0B1

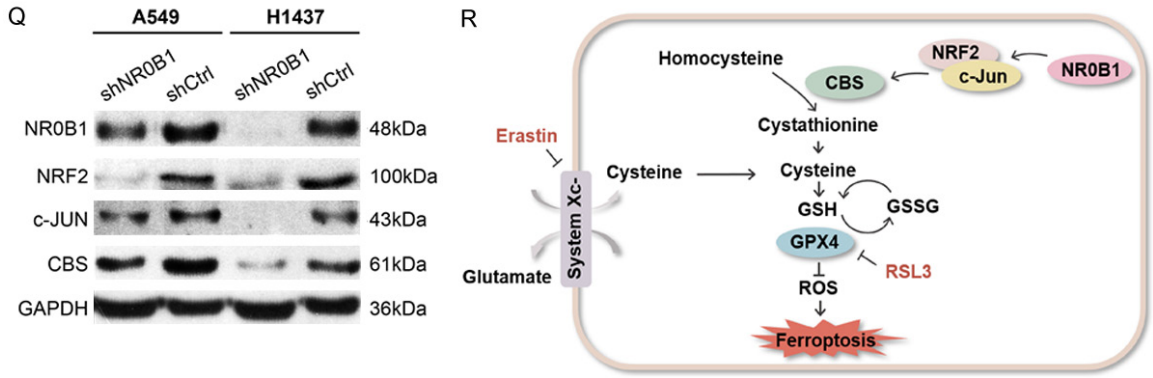

Figure 8. NR0B1-depletion restrains the tumor growth and facilitates RSL3-induced ferroptosis. (A, B) Representative subcutaneous tumors from mice implanted with NR0B1-KD cells of A549 (A) and H1437 (B). (C, D) The xenografts sizes of (A and B). (E, F) The xenografts weight of (A and B). (G, H) Representative subcutaneous tumors from mice implanted with NR0B1-KD cells of A549 (G) and H1437 (H) after the treatment with RSL3. (I, J) The xenografts sizes of (G and H). (K, L) The xenografts weight of (G and H). (M, N) Relative MDA level changes in (G and H) xenografts. (O, P) Relative iron level changes in (G and H) xenografts. (Q) The protein levels of NRF2, c-JUN and CBS in (G and H) xenografts. (R) Schematic depiction of the mechanisms underlying inhibition of ferroptosis by NR0B1 through NRF2/c-JUN-CBS signaling. Data are presented as mean ± SD, n = 3, $*P < 0.05$, $**P < 0.01$, $***P < 0.001$.

geted genes are implicated in the development of tumor drug resistance, and treatments targeting these nuclear receptors may provide new avenues to mitigate, or even prevent, drug resistance. NR0B1, as a member of the nuclear receptor superfamily, has been reported to enhance resistance to chemotherapeutic agents such as cisplatin and topotecan [22, 25]. In this study, we identified that NR0B1 reduced the sensitivity of lung cancer cells to erastin and RSL3-induced ferroptosis. Our additional study also revealed that NR0B1 enhanced the survivability of hepatocellular cancer cells treated with sorafenib (data not shown). These findings suggest that NR0B1 may be a target for overcoming MDR in cancer treatment.

CBS, acting as an essential component in the trans-sulfuration pathway, converts homocysteine to cysteine, a crucial precursor for glutathione [36]. CBS-mediated ferroptosis resistance has been found in many cancers, such as liver [36], breast [59] and ovarian [45] cancers, and neuroblastoma [60]. Recently, some factors such as c-JUN, NRF2 [35, 45] and non-coding RNAs [13, 61], have been observed to regulate ferroptosis by controlling CBS activity in cancer cells. Moreover, CBS inhibitors have been identified to facilitate antitumor effects [62]. In the present study, we found that NR0B1 suppressed ferroptosis through promoting NRF2/c-JUN-mediated CBS expression in lung cancer cells, and the CBS inhibitor AOAA circumvented the NR0B1 repression on ferroptosis. Although these findings support future targeted cancer therapies based on pharmacological CBS inhibition, the controversial roles of CBS in human cancers should be considered. In some cancers, such as glioma [63] and hepatocellular carcinoma [64], CBS is demonstrated to suppress tumorigenicity. Therefore, more tumor type-specific investigations of CBS function are necessary prior to CBS-based targeted therapies.

In conclusion, our study unveils a unique role for NR0B1 in suppressing ferroptosis in lung cancer cells. NR0B1 enhances ferroptosis resistance through promoting CBS expression driven by NRF2/c-JUN upregulation. Our findings provided new insights indicating that NR0B1 is involved in drug resistance during cancer therapy.

Acknowledgements

We thank the staff of the Laboratory Animal Center and the Research Core Facility, West China Hospital, Sichuan University, China, for their assistance in mouse handling and instrument operation. This work was supported by Grants from the National Natural Science Foundation of China (81773159 and 81871-203), and the Sichuan Science and Technology Program (2022NSFSC0679).

Disclosure of conflict of interest

None.

Address correspondence to: Yuan Yang and Yun-Qiang Liu, Department of Medical Genetics and State Key Laboratory of Biotherapy, West China Hospital, Sichuan University, Chengdu 610041, Sichuan, China. E-mail: yangyuan@scu.edu.cn (YY); yq_liu@scu.edu.cn (YQL)

References

[1] Siegel RL, Miller KD, Wagle NS and Jemal A. Cancer statistics, 2023. CA Cancer J Clin 2023; 73: 17-48.

[2] Lim ZF and Ma PC. Emerging insights of tumor heterogeneity and drug resistance mechanisms in lung cancer targeted therapy. J Hematol Oncol 2019; 12: 134.

[3] Stockwell BR. Ferroptosis turns 10: emerging mechanisms, physiological functions, and therapeutic applications. Cell 2022; 185: 2401-2421.

[4] Zhang C, Liu X, Jin S, Chen Y and Guo R. Ferroptosis in cancer therapy: a novel approach to reversing drug resistance. Mol Cancer 2022; 21: 47.

[5] Freire Boullosa L, Van Loenhout J, Flieswasser T, De Waele J, Hermans C, Lambrechts H, Cuypers B, Laukens K, Bartholomeus E, Siozopoulou V, De Vos WH, Peeters M, Smits ELJ and Deben C. Auranofin reveals therapeutic anticancer potential by triggering distinct molecular cell death mechanisms and innate immunity in mutant p53 non-small cell lung cancer. Redox Biol 2021; 42: 101949.

[6] Zhang R, Pan T, Xiang Y, Zhang M, Xie H, Liang Z, Chen B, Xu C, Wang J, Huang X, Zhu Q, Zhao Z, Gao Q, Wen C, Liu W, Ma W, Feng J, Sun X, Duan T, Lai-Han Leung E, Xie T, Wu Q and Sui X. Curcumenol triggered ferroptosis in lung cancer cells via lncRNA H19/miR-19b-3p/FTH1 axis. Bioact Mater 2021; 13: 23-36.

[7] Wang L, Fu H, Song L, Wu Z, Yu J, Guo Q, Chen C, Yang X, Zhang J, Wang Q, Duan Y and Yang Y. Overcoming AZD9291 resistance and metastasis of NSCLC via ferroptosis and multitarget interference by nanocatalytic sensitizer plus AHP-DRI-12. Small 2023; 19: e2204133.

[8] Alvarez SW, Sviderskiy VO, Terzi EM, Papagiannakopoulos T, Moreira AL, Adams S, Sabatini DM, Birsoy K and Possemato R. NFS1 undergoes positive selection in lung tumours and protects cells from ferroptosis. Nature 2017; 551: 639-643.

[9] Wang X, Chen Y, Wang X, Tian H, Wang Y, Jin J, Shan Z, Liu Y, Cai Z, Tong X, Luan Y, Tan X, Luan B, Ge X, Ji H, Jiang X and Wang P. Stem cell factor SOX2 confers ferroptosis resistance in lung cancer via upregulation of SLC7A11. Cancer Res 2021; 81: 5217-5229.

[10] Zhang W, Sun Y, Bai L, Zhi L, Yang Y, Zhao Q, Chen C, Qi Y, Gao W, He W, Wang L, Chen D, Fan S, Chen H, Piao HL, Qiao Q, Xu Z, Zhang J, Zhao J, Zhang S, Yin Y, Peng C, Li X, Liu Q, Liu H and Wang Y. RBMS1 regulates lung cancer ferroptosis through translational control of SLC7A11. J Clin Invest 2021; 131: e152067.

[11] Bebber CM, Thomas ES, Stroh J, Chen Z, Androulidaki A, Schmitt A, Hohne MN, Stuker L, de Padua Alves C, Khonsari A, Dammert MA, Parmaksiz F, Tumbrink HL, Beleggia F, Sos ML, Riemer J, George J, Brodesser S, Thomas RK, Reinhardt HC and von Karstedt S. Ferroptosis response segregates small cell lung cancer (SCLC) neuroendocrine subtypes. Nat Commun 2021; 12: 2048.

[12] Mao C, Wang X, Liu Y, Wang M, Yan B, Jiang Y, Shi Y, Shen Y, Liu X, Lai W, Yang R, Xiao D, Cheng Y, Liu S, Zhou H, Cao Y, Yu W, Muegge K, Yu H and Tao Y. A G3BP1-interacting lncRNA promotes ferroptosis and apoptosis in cancer via nuclear sequestration of p53. Cancer Res 2018; 78: 3484-3496.

[13] Wang M, Mao C, Ouyang L, Liu Y, Lai W, Liu N, Shi Y, Chen L, Xiao D, Yu F, Wang X, Zhou H, Cao Y, Liu S, Yan Q, Tao Y and Zhang B. Long noncoding RNA LINC00336 inhibits ferroptosis in lung cancer by functioning as a competing endogenous RNA. Cell Death Differ 2019; 26: 2329-2343.

[14] Suntharalingham JP, Buonocore F, Duncan AJ and Achermann JC. DAX-1 (NR0B1) and steroidogenic factor-1 (SF-1, NR5A1) in human disease. Best Pract Res Clin Endocrinol Metab 2015; 29: 607-619.

[15] Kelly VR, Xu B, Kuick R, Koenig RJ and Hammer GD. Dax1 up-regulates Oct4 expression in mouse embryonic stem cells via LRH-1 and SRA. Mol Endocrinol 2010; 24: 2281-2291.

[16] Kim J, Chu J, Shen X, Wang J and Orkin SH. An extended transcriptional network for pluripotency of embryonic stem cells. Cell 2008; 132: 1049-1061.

[17] Zhang J, Liu G, Ruan Y, Wang J, Zhao K, Wan Y, Liu B, Zheng H, Peng T, Wu W, He P, Hu FQ and Jian R. Dax1 and Nanog act in parallel to stabilize mouse embryonic stem cells and induced pluripotency. Nat Commun 2014; 5: 5042.

[18] Swain A, Narvaez V, Burgoyne P, Camerino G and Lovell-Badge R. Dax1 antagonizes Sry action in mammalian sex determination. Nature 1998; 391: 761-767.

[19] Muscatelli F, Strom TM, Walker AP, Zanaria E, Recan D, Meindl A, Bardoni B, Guioli S, Zehet-

ner G, Rabl W, et al. Mutations in the DAX-1 gene give rise to both X-linked adrenal hypoplasia congenita and hypogonadotropic hypogonadism. Nature 1994; 372: 672-676.
[20] Garcia-Aragoncillo E, Carrillo J, Lalli E, Agra N, Gomez-Lopez G, Pestana A and Alonso J. DAX1, a direct target of EWS/FLI1 oncoprotein, is a principal regulator of cell-cycle progression in Ewing's tumor cells. Oncogene 2008; 27: 6034-6043.
[21] Conde I, Alfaro JM, Fraile B, Ruiz A, Paniagua R and Arenas MI. DAX-1 expression in human breast cancer: comparison with estrogen receptors ER-alpha, ER-beta and androgen receptor status. Breast Cancer Res 2004; 6: R140-148.
[22] Liu XF, Li XY, Zheng PS and Yang WT. DAX1 promotes cervical cancer cell growth and tumorigenicity through activation of Wnt/beta-catenin pathway via GSK3beta. Cell Death Dis 2018; 9: 339.
[23] Abd-Elaziz M, Akahira J, Moriya T, Suzuki T, Yaegashi N and Sasano H. Nuclear receptor DAX-1 in human common epithelial ovarian carcinoma: an independent prognostic factor of clinical outcome. Cancer Sci 2003; 94: 980-985.
[24] Nakamura Y, Suzuki T, Arai Y and Sasano H. Nuclear receptor DAX1 in human prostate cancer: a novel independent biological modulator. Endocr J 2009; 56: 39-44.
[25] Oda T, Tian T, Inoue M, Ikeda J, Qiu Y, Okumura M, Aozasa K and Morii E. Tumorigenic role of orphan nuclear receptor NR0B1 in lung adenocarcinoma. Am J Pathol 2009; 175: 1235-1245.
[26] Lu Y, Liu Y, Liao S, Tu W, Shen Y, Yan Y, Tao D, Lu Y, Ma Y, Yang Y and Zhang S. Epigenetic modifications promote the expression of the orphan nuclear receptor NR0B1 in human lung adenocarcinoma cells. Oncotarget 2016; 7: 43162-43176.
[27] Koppula P, Zhuang L and Gan B. Cystine transporter SLC7A11/xCT in cancer: ferroptosis, nutrient dependency, and cancer therapy. Protein Cell 2021; 12: 599-620.
[28] Seibt TM, Proneth B and Conrad M. Role of GPX4 in ferroptosis and its pharmacological implication. Free Radic Biol Med 2019; 133: 144-152.
[29] Bar-Peled L, Kemper EK, Suciu RM, Vinogradova EV, Backus KM, Horning BD, Paul TA, Ichu TA, Svensson RU, Olucha J, Chang MW, Kok BP, Zhu Z, Ihle NT, Dix MM, Jiang P, Hayward MM, Saez E, Shaw RJ and Cravatt BF. Chemical proteomics identifies druggable vulnerabilities in a genetically defined cancer. Cell 2017; 171: 696-709, e23.
[30] Sporn MB and Liby KT. NRF2 and cancer: the good, the bad and the importance of context. Nat Rev Cancer 2012; 12: 564-571.
[31] Sun X, Ou Z, Chen R, Niu X, Chen D, Kang R and Tang D. Activation of the p62-Keap1-NRF2 pathway protects against ferroptosis in hepatocellular carcinoma cells. Hepatology 2016; 63: 173-184.
[32] Venugopal R and Jaiswal AK. Nrf2 and Nrf1 in association with Jun proteins regulate antioxidant response element-mediated expression and coordinated induction of genes encoding detoxifying enzymes. Oncogene 1998; 17: 3145-3156.
[33] Wang L, Liu Y, Du T, Yang H, Lei L, Guo M, Ding HF, Zhang J, Wang H, Chen X and Yan C. ATF3 promotes erastin-induced ferroptosis by suppressing system Xc. Cell Death Differ 2020; 27: 662-675.
[34] Kremer DM, Nelson BS, Lin L, Yarosz EL, Halbrook CJ, Kerk SA, Sajjakulnukit P, Myers A, Thurston G, Hou SW, Carpenter ES, Andren AC, Nwosu ZC, Cusmano N, Wisner S, Mbah NE, Shan M, Das NK, Magnuson B, Little AC, Savani MR, Ramos J, Gao T, Sastra SA, Palermo CF, Badgley MA, Zhang L, Asara JM, McBrayer SK, di Magliano MP, Crawford HC, Shah YM, Olive KP and Lyssiotis CA. GOT1 inhibition promotes pancreatic cancer cell death by ferroptosis. Nat Commun 2021; 12: 4860.
[35] Chen Y, Zhu G, Liu Y, Wu Q, Zhang X, Bian Z, Zhang Y, Pan Q and Sun F. O-GlcNAcylated c-Jun antagonizes ferroptosis via inhibiting GSH synthesis in liver cancer. Cell Signal 2019; 63: 109384.
[36] Hayano M, Yang WS, Corn CK, Pagano NC and Stockwell BR. Loss of cysteinyl-tRNA synthetase (CARS) induces the transsulfuration pathway and inhibits ferroptosis induced by cystine deprivation. Cell Death Differ 2016; 23: 270-278.
[37] Hou W, Xie Y, Song X, Sun X, Lotze MT, Zeh HJ 3rd, Kang R and Tang D. Autophagy promotes ferroptosis by degradation of ferritin. Autophagy 2016; 12: 1425-1428.
[38] Sun X, Ou Z, Xie M, Kang R, Fan Y, Niu X, Wang H, Cao L and Tang D. HSPB1 as a novel regulator of ferroptotic cancer cell death. Oncogene 2015; 34: 5617-5625.
[39] Kwon MY, Park E, Lee SJ and Chung SW. Heme oxygenase-1 accelerates erastin-induced ferroptotic cell death. Oncotarget 2015; 6: 24393-24403.
[40] Ou Y, Wang SJ, Li D, Chu B and Gu W. Activation of SAT1 engages polyamine metabolism with p53-mediated ferroptotic responses. Proc Natl Acad Sci U S A 2016; 113: E6806-E6812.

[41] McGivan JD and Bungard CI. The transport of glutamine into mammalian cells. Front Biosci 2007; 12: 874-882.
[42] Gagliardi M, Cotella D, Santoro C, Cora D, Barlev NA, Piacentini M and Corazzari M. Aldo-keto reductases protect metastatic melanoma from ER stress-independent ferroptosis. Cell Death Dis 2019; 10: 902.
[43] Dixon SJ, Lemberg KM, Lamprecht MR, Skouta R, Zaitsev EM, Gleason CE, Patel DN, Bauer AJ, Cantley AM, Yang WS, Morrison B 3rd and Stockwell BR. Ferroptosis: an iron-dependent form of nonapoptotic cell death. Cell 2012; 149: 1060-1072.
[44] Vogt PK. Jun, the oncoprotein. Oncogene 2001; 20: 2365-2377.
[45] Liu N, Lin X and Huang C. Activation of the reverse transsulfuration pathway through NRF2/CBS confers erastin-induced ferroptosis resistance. Br J Cancer 2020; 122: 279-292.
[46] Garcia-Mayea Y, Mir C, Masson F, Paciucci R and LLeonart ME. Insights into new mechanisms and models of cancer stem cell multidrug resistance. Semin Cancer Biol 2020; 60: 166-180.
[47] Jiang X, Stockwell BR and Conrad M. Ferroptosis: mechanisms, biology and role in disease. Nat Rev Mol Cell Biol 2021; 22: 266-282.
[48] Yang FC, Wang C, Zhu J, Gai QJ, Mao M, He J, Qin Y, Yao XX, Wang YX, Lu HM, Cao MF, He MM, Wen XM, Leng P, Cai XW, Yao XH, Bian XW and Wang Y. Inhibitory effects of temozolomide on glioma cells is sensitized by RSL3-induced ferroptosis but negatively correlated with expression of ferritin heavy chain 1 and ferritin light chain. Lab Invest 2022; 102: 741-752.
[49] Chen L, Li X, Liu L, Yu B, Xue Y and Liu Y. Erastin sensitizes glioblastoma cells to temozolomide by restraining xCT and cystathionine-gamma-lyase function. Oncol Rep 2015; 33: 1465-1474.
[50] Li M, Chen X, Wang X, Wei X, Wang D, Liu X, Xu L, Batu W, Li Y, Guo B and Zhang L. RSL3 enhances the antitumor effect of cisplatin on prostate cancer cells via causing glycolysis dysfunction. Biochem Pharmacol 2021; 192: 114741.
[51] Li Y, Yan H, Xu X, Liu H, Wu C and Zhao L. Erastin/sorafenib induces cisplatin-resistant non-small cell lung cancer cell ferroptosis through inhibition of the Nrf2/xCT pathway. Oncol Lett 2020; 19: 323-333.
[52] Chang MT, Tsai LC, Nakagawa-Goto K, Lee KH and Shyur LF. Phyto-sesquiterpene lactones DET and DETD-35 induce ferroptosis in vemurafenib sensitive and resistant melanoma via GPX4 inhibition and metabolic reprogramming. Pharmacol Res 2022; 178: 106148.
[53] Tsoi J, Robert L, Paraiso K, Galvan C, Sheu KM, Lay J, Wong DJL, Atefi M, Shirazi R, Wang X, Braas D, Grasso CS, Palaskas N, Ribas A and Graeber TG. Multi-stage differentiation defines melanoma subtypes with differential vulnerability to drug-induced iron-dependent oxidative stress. Cancer Cell 2018; 33: 890-904, e5.
[54] Gout PW, Buckley AR, Simms CR and Bruchovsky N. Sulfasalazine, a potent suppressor of lymphoma growth by inhibition of the x(c)- cystine transporter: a new action for an old drug. Leukemia 2001; 15: 1633-1640.
[55] Louandre C, Ezzoukhry Z, Godin C, Barbare JC, Maziere JC, Chauffert B and Galmiche A. Iron-dependent cell death of hepatocellular carcinoma cells exposed to sorafenib. Int J Cancer 2013; 133: 1732-1742.
[56] von Hagens C, Walter-Sack I, Goeckenjan M, Osburg J, Storch-Hagenlocher B, Sertel S, Elsasser M, Remppis BA, Edler L, Munzinger J, Efferth T, Schneeweiss A and Strowitzki T. Prospective open uncontrolled phase I study to define a well-tolerated dose of oral artesunate as add-on therapy in patients with metastatic breast cancer (ARTIC M33/2). Breast Cancer Res Treat 2017; 164: 359-369.
[57] Miranda Furtado CL, Dos Santos Luciano MC, Silva Santos RD, Furtado GP, Moraes MO and Pessoa C. Epidrugs: targeting epigenetic marks in cancer treatment. Epigenetics 2019; 14: 1164-1176.
[58] Chen Y, Tang Y, Guo C, Wang J, Boral D and Nie D. Nuclear receptors in the multidrug resistance through the regulation of drug-metabolizing enzymes and drug transporters. Biochem Pharmacol 2012; 83: 1112-1126.
[59] Erdelyi K, Ditroi T, Johansson HJ, Czikora A, Balog N, Silwal-Pandit L, Ida T, Olasz J, Hajdu D, Matrai Z, Csuka O, Uchida K, Tovari J, Engebraten O, Akaike T, Borresen Dale AL, Kasler M, Lehtio J and Nagy P. Reprogrammed transsulfuration promotes basal-like breast tumor progression via realigning cellular cysteine persulfidation. Proc Natl Acad Sci U S A 2021; 118: e2100050118.
[60] Floros KV, Chawla AT, Johnson-Berro MO, Khatri R, Stamatouli AM, Boikos SA, Dozmorov MG, Cowart LA and Faber AC. MYCN upregulates the transsulfuration pathway to suppress the ferroptotic vulnerability in MYCN-amplified neuroblastoma. Cell Stress 2022; 6: 21-29.
[61] Yang H, Hu Y, Weng M, Liu X, Wan P, Hu Y, Ma M, Zhang Y, Xia H and Lv K. Hypoxia inducible lncRNA-CBSLR modulates ferroptosis through m6A-YTHDF2-dependent modulation of CBS in gastric cancer. J Adv Res 2021; 37: 91-106.
[62] Zuhra K, Augsburger F, Majtan T and Szabo C. Cystathionine-beta-synthase: molecular regu-

lation and pharmacological inhibition. Biomolecules 2020; 10: 697.
[63] Takano N, Sarfraz Y, Gilkes DM, Chaturvedi P, Xiang L, Suematsu M, Zagzag D and Semenza GL. Decreased expression of cystathionine beta-synthase promotes glioma tumorigenesis. Mol Cancer Res 2014; 12: 1398-1406.
[64] Zhou YF, Song SS, Tian MX, Tang Z, Wang H, Fang Y, Qu WF, Jiang XF, Tao CY, Huang R, Zhou PY, Zhu SG, Zhou J, Fan J, Liu WR and Shi YH. Cystathionine beta-synthase mediated PRRX2/IL-6/STAT3 inactivation suppresses Tregs infiltration and induces apoptosis to inhibit HCC carcinogenesis. J Immunother Cancer 2021; 9: e003031.

Table S1. The sequences of plasmid constructions

Sequence name	Forward (5' -> 3')	Description	References
shNR0B1	GGGAACTCAGCAAATACTCAGTGAA		[1]
shNRF2	TGAAAGCACAGCAGAATT		[2, 3]
sh c-JUN	AACCTCAGCAACTTCAACCCA		[4, 5]
siCBS	CCAAGUGUGAGUUCUUCAA dTdT		[6, 7]
NR0B1-rescue	ggatccgccacc**ATG**gcgggcgagaaccaccagtggcagggcagcatcctctacaacatgcttatgagcgcgaagcaaacgcgcgcggctcctgag-gctccagagacgcggctggtggatcagtgctggggctgttcgtgcggcgatgagcccggggtgggcagagaggggctgctgggcgggcggaacgtggc-gctcctgtaccgctgctgcttttgcggtaaagaccacccacggcagggcagcatcctctacagcatgctgacgagcgcaaagcaaacgtacgcggcac-cgaaggcgcccgaggcgacgctgggtccgtgctggggctgttcgtgcggctctgatcccggggtgggcagagcggggcttccgggtgggcggcccgtg-gcactcctgtaccgctgctgcttttgtggtgaagaccacccgcggcagggcagcatcctctacagcttgctcactagctcaaagcaaacgcacgtggctcc-ggcagcgcccgaggcacggccaggggcgcgtggtgggaccgctcctacttcgcgcagaggccaggggtaaagaggcgctaccaggcgggcgggc-cacggcgcttctgtaccgctgctgcttttgcggtgaagaccacccgcagcagggcagcaccctctactgcgtgcccacgagcacaaatcaagcgcag-gcggctccggaggagcggccgagggcccccctggtgggacacctcctctggtgcgctgcggccggtggcgctcaagagtccacaggtggtctgcgag-gcagcctcagcgggcctgttgaagacgctgcgcttcgtcaagtacttgccctgcttccaggtgctgcccctggaccagcagctggtgctggtgcgcaact-gctgggcgtccctgctcatgcttgagctggcccaggaccgcttgcagttcgagactgtggaagtctcggagcccagcatgctgcagaagatcctcaccac-caggcggcgggagaccgggggcaacgagccactgcccgtgcccacgctgcagcaccatttggcaccgccggcggaggccaggaaggtgccctc-cgcctcccaggtccaagccatcaagtgctttctttccaaatgctggagtctgaacatcagtaccaaggagtacgcctacctcaaggggaccgtgctctt-taacccggacgtgccgggcctgcagtgcgtgaagtacattcagggactccag**TGGGGCACCCAACAGATCTTGTCCGAG**cacaccaggat-gacgcaccaagggccccatgacagattcatcgaacttaatagtacccttttcctgctgagattcatcaatgccaatgtcattgctgaactgttcttcag-gcccatcatcggcacagtcagcatggatgatatgatgctggaaatgctctgtacaaagata**TGCCAAGATCCTCAACGCAAAGGCAACGT-GATACTCTCTCAGGCTTACGGGTGCCAAGATCCTCAACGCAAAGGCAACGTGATACTCTCTCAGGCTTAC**TAG**gaattc	The bolded part indicates the promoter and termination codon. The red part indicates the part of NR0B1-rescue sequence after the shNR0B1 sequence has been modified according to codon degeneracy. The yellow part indicates the AM-Tag sequence.	

References

[1] Bar-Peled L, Kemper EK, Suciu RM, Vinogradova EV, Backus KM, Horning BD, Paul TA, Ichu TA, Svensson RU, Olucha J, Chang MW, Kok BP, Zhu Z, Ihle NT, Dix MM, Jiang P, Hayward MM, Saez E, Shaw RJ and Cravatt BF. Chemical Proteomics Identifies Druggable Vulnerabilities in a Genetically Defined Cancer. Cell 2017; 171: 696-709, e623.

[2] Fourtounis J, Wang IM, Mathieu MC, Claveau D, Loo T, Jackson AL, Peters MA, Therien AG, Boie Y and Crackower MA. Gene expression profiling following NRF2 and KEAP1 siRNA knockdown in human lung fibroblasts identifies CCL11/Eotaxin-1 as a novel NRF2 regulated gene. Respir Res 2012; 13: 92.

[3] Ni S, Qian Z, Yuan Y, Li D, Zhong Z, Ghorbani F, Zhang X, Zhang F, Zhang Z, Liu Z and Yu B. Schisandrin A restrains osteoclastogenesis by inhibiting reactive oxygen species and activating Nrf2 signalling. Cell Prolif 2020; 53: e12882.

[4] Zhou C, Martinez E, Di Marcantonio D, Solanki-Patel N, Aghayev T, Peri S, Ferraro F, Skorski T, Scholl C, Frohling S, Balachandran S, Wiest DL and Sykes SM. JUN is a key transcriptional regulator of the unfolded protein response in acute myeloid leukemia. Leukemia 2017; 31: 1196-1205.

[5] Snyder EL, Sandstrom DJ, Law K, Fiore C, Sicinska E, Brito J, Bailey D, Fletcher JA, Loda M, Rodig SJ, Dal Cin P and Fletcher CD. c-Jun amplification and overexpression are oncogenic in liposarcoma but not always sufficient to inhibit the adipocytic differentiation programme. J Pathol 2009; 218: 292-300.

[6] Duan X, Pan L, Deng Y, Liu Y, Han X, Fu H, Li Y, Li M and Wang T. Dandelion root extract affects ESCC progression via regulating multiple signal pathways. Food Funct 2021; 12: 9486-9502.

[7] Yan J, Teng F, Chen W, Ji Y and Gu Z. Cystathionine beta-synthase-derived hydrogen sulfide regulates lipopolysaccharide-induced apoptosis of the BRL rat hepatic cell line in vitro. Exp Ther Med 2012; 4: 832-838.

Table S2. Primers for amplification of promoter fragments with different lengths of NRF2, c-JUN and CBS

Primer name	Forward (5' -> 3')	Description
c-JUN FL-F	ATTTCTCTATCGATAGGTACCGGAATGTAACACAGACCTGAGG	Amplification primers designed according to NR0B1 binding elements (NREs) in the *c-JUN* promoter region.
c-JUN P1-F	ATTTCTCTATCGATAGGTACCAGCGCTTCCTAGAGGCTAC	
c-JUN P2-F	ATTTCTCTATCGATAGGTACCCAGTTTCGGGCAATACAAA	
c-JUN P3-F	ATTTCTCTATCGATAGGTACCCGCCGGTGGATGACTTC	
c-JUN UR	ACTTAGATCGCAGATCTCGAGCACGGGATGAGGTAATGCT	
NRF2 FL-F	ATTTCTCTATCGATAGGTACCTACACATAAATCCTGGGAGTGTC	Amplification primers designed according to NREs in the *NRF2* promoter region.
NRF2 P1-F	ATTTCTCTATCGATAGGTACCTTTTGTGAGTACGTGAAAAAGA	
NRF2 P2-F	ATTTCTCTATCGATAGGTACCAGGGAGGAGCGCCTTAAGT	
NRF2 UR	ACTTAGATCGCAGATCTCGAGCGAGGTTTGCACGCTATAA	
CBS FL-F	CTGGCCGGTACCGCTAGCCTCGAGCCAGGATGGTCTCAATCTCTTGA	Amplification primers designed according to the *CBS* promoter region from -2640bp to +231bp.
CBS FL-R	CAACAGTACCGGATTGCCAAGCTTGGTGTTCCGATGCTGTTTTACTT	
CBS-NR0B1 P1-F	AGAACATTTCTCTATCGATAGGTACCTTGGAAAATCTGGATGAGGGAA	Amplification primers designed according to NREs in the *CBS* promoter region.
CBS-NR0B1 P1-R	TTGAGATGCAGATCGCAGATCTCGAGTCCGATGCTGTTTTACTTGGTT	
CBS-NR0B1 P2-F	AGAACATTTCTCTATCGATAGGTACCACAGTCTCGCTCAGTCGCAC	
CBS-NR0B1 P2-R	TTGAGATGCAGATCGCAGATCTCGAGCAAGATTTTTGGAGATTTTGCCG	
CBS-c-JUN/NRF2 P1-F	AGAACATTTCTCTATCGATAGGTACCTGGAAAATCTGGATGAGGGAAT	Amplification primers designed according to the antioxidant response elements (AREs) in the *CBS* promoter region.
CBS-c-JUN/NRF2 P1-R	TTGAGATGCAGATCGCAGATCTCGAGGGGATTACAGGCACGCACC	
CBS-c-JUN/NRF2 P2-F	AGAACATTTCTCTATCGATAGGTACCTGTGAGCCTAGCACTTTTGGGAG	
CBS-c-JUN/NRF2 P2-R	TTGAGATGCAGATCGCAGATCTCGAGGGATTACAGGCACGCACCACC	

Table S3. Primers for RT-qPCR

Primer name	Forward (5' -> 3')	Reverse (5' -> 3')
NR0B1	CATCAAGTGCTTTCTTTCCA	TGAGTATTTGCTGAGTTCCC
c-JUN	GGGAAGTGAGTTCGCCTGC	GATGCCTCCCGCACTCTTACT
NRF2	CCCAGCACATCCAGTCAGAA	CGTAGCCGAAGAAACCTCATT
CBS	AAGGAAGCCAAGGAGCCC	GCCGAACTTCTTCCCAATC
GAPDH	ACGGATTTGGTCGTATTGGG	CGCTCCTGGAAGATGGTGAT

Table S4. The list of antibodies used in this study

Antibody name	Catalogue number	Specificity	Manufacturer
NR0B1	#13538	Rabbit monoclonal	Cell Signaling Technology
SLC7A11	26864-1-AP	Rabbit Polyclonal	Proteintech
GPX4	14432-1-AP	Rabbit Polyclonal	Proteintech
c-JUN	#9165	Rabbit monoclonal	Cell Signaling Technology
NRF2	16396-1-AP	Rabbit Polyclonal	Proteintech
CBS	14787-1-AP	Rabbit Polyclonal	Proteintech
IgG	#3900	Rabbit monoclonal	Cell Signaling Technology
AM-Tag	#61677	Rabbit Polyclonal	Active Motif

Table S5. The list of primers used for ChIP-PCR

Primer name	Forward (5' -> 3')
c-JUN ChIP F1	TATTTAGAACACCAACTCCCTG
c-JUN ChIP R1	AGATCCAGTTGCTTCCTCAA
c-JUN ChIP F2	TACTACTGCGTGACTTTATGCGA
c-JUN ChIP R2	GCACACACACACTCCATCCG
c-JUN ChIP F3	TGGGACTTCACAGAGCCACCTT
c-JUN ChIP R3	TGAGAATCCAAGTACGCTGCCA
NRF2 ChIP F1	CATAAAACATACGCACTGCAGAT
NRF2 ChIP R1	AAATGCTGTGGAATCAACGA
NRF2 ChIP F2	GGGCTTCTCCGTTTGCCTTTG
NRF2 ChIP R2	GAACGCCCTCCTCTGAACTCCC
NRF2 ChIP F3	GGCTTTGCGAAGTCATCCAT
NRF2 ChIP R3	TGGGCTTTCAAGAGAGCTCAA
CBS-NRE ChIP F1	GCGTAGTGCTCCAGTTCTC
CBS-NRE ChIP R1	GAAACCTCGCCTCTACTA
CBS-NRE ChIP F2	TCTTTACCGTCCCTACCG
CBS-NRE ChIP R2	CCTCCCTCAGAGCCTTC
CBS-NRE ChIP F3	GTCGTGGCGAGTTTGAGA
CBS-NRE ChIP R3	TGGTGTTCCGATGCTGTT
CBS-ARE ChIP F1	AGGTTGCAGTGAGCTGAAAT
CBS-ARE ChIP R1	TTTTGAGACAGAATCTTTCTCTG
CBS-ARE ChIP F2	ACCTGATGTTAGGGGTTCGA
CBS-ARE ChIP R2	TTTAGTAGAGACGGGGTTTCATC
CBS-ARE ChIP F3	AATGCCACCTTCCAGAGCCT
CBS-ARE ChIP R3	GGCAGGAACTGACACGAAGAAC

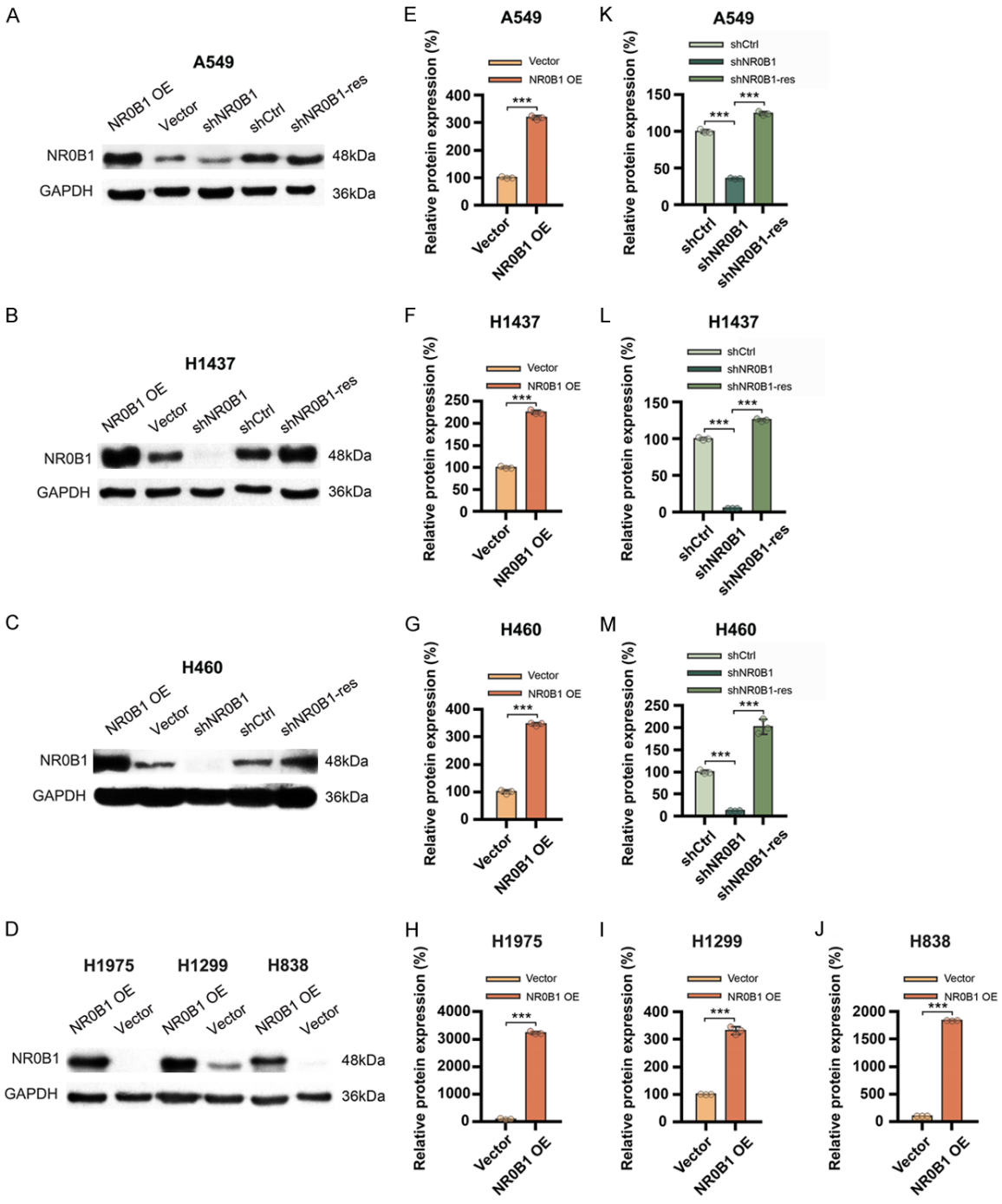

Figure S1. Construction of cellular models with different expression levels of NR0B1. Six lung cancer cell lines including A549, H1437, H460, H1975, H1299 and H838 were selected to generate the cellular models with stable exogenous overexpression (OE) of NR0B1 and the models with down-regulated NR0B1 (shNR0B1). Additionally, the models with rescued NR0B1 expression (shNR0B1-res) were also constructed by overexpressing shRNA-resistant NR0B1 mutant carrying an 11-nt mismatch to the shNR0B1 sequence. A-D. Western blotting showed the protein levels of NR0B1 in different cell models. E-J. The relative protein levels of NR0B1 (versus GAPDH) in the NR0B1-overexpression cell models. K-M. The relative protein levels of NR0B1 in the NR0B1-knock down and -rescue cell models. The protein levels of GAPDH were used as an internal control and the relative NR0B1 protein levels (versus GAPDH) were calculated using Image J software. Data are presented as mean ± SD, $*P < 0.05$, $**P < 0.01$, $***P < 0.001$.

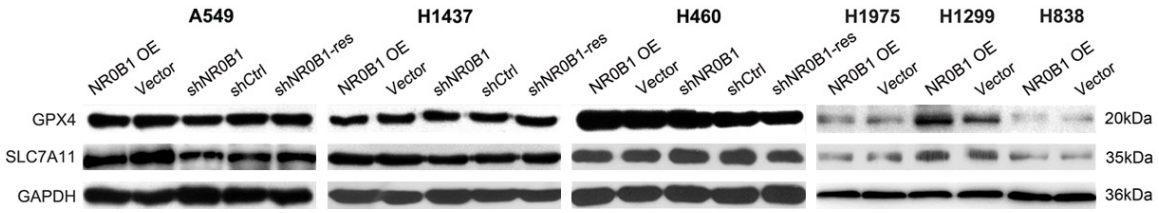

Figure S2. The protein levels of GPX4 and system X_c^- in lung cancer cells with different expression levels of NR0B1.

Table S6. Different expression genes(DEGs) in NR0B1 OE cells

up-regulated DEGs	log2(FC)	FDR	down-regulated DEGs	log2(FC)	FDR
AADAC	1.9123245	5.83E-06	ACADVL	-1.088053	0.0361912
ABCC2	1.4832397	0.0409922	ACER2	-10.35902	0.0120548
ABL2	2.5413591	7.09E-05	ACO1	-1.134176	0.0486923
ADM	2.2433735	0.0001531	ACOX2	-9.829723	0.019206
ADPRHL1	3.3429897	0.0040965	ACVR1	-10.73697	0.0074047
AFAP1	2.3345404	0.0014215	ADCY7	-10.35168	0.0319842
AHDC1	9.7256503	0.0262899	ADGRB2	-9.329423	0.0046403
AHRR	1.88168	0.0141755	ADGRG2	-9.941537	0.035031
AJUBA	1.1860335	0.0459394	AGPAT1	-11.07236	0.0006658
ALPK2	2.6731203	1.03E-09	AKR1B1	-1.133529	0.0426305
AMD1	1.6414371	0.0389477	APBB3	-10.44087	0.0116927
AMOTL2	1.8746922	6.41E-07	ARAP1	-10.35168	0.0221113
ANKRD1	4.024687	6.77E-13	ARF3	-11.21067	0.0494418
ANKRD40	3.5878918	0.0430756	ARHGEF2	-10.46148	0.0199225
AP2B1	9.8765169	0.0003502	ARHGEF37	-9.451211	0.017437
AP2S1	11.951285	0.0097783	ARL4D	-2.079168	0.0480236
APOL2	9.6794801	0.026314	ARRDC3	-1.250854	0.0171249
ARHGAP11A	1.2561074	0.0427939	ASUN	-11.28193	0.0133355
ARID2	9.3663222	0.0400812	BACH1	-9.965784	0.0292015
ATXN7L2	6.3966048	0.0040637	BICD1	-5.411814	0.0077291
B3GALT5	1.5412146	0.0345323	BIRC3	-1.236014	0.0152097
BCAR1	5.8302233	0.0047207	BRD8	-1.547609	0.0223731
BCAR3	2.5620361	0.0311031	BRSK1	-10.12498	0.029274
BCL2L11	8.3808218	0.0485002	BTAF1	-9.531381	0.027102
BCLAF1	1.6984601	0.0078157	BTG2	-1.560426	0.017437
BCOR	10.264443	0.0262734	BTRC	-11.11634	0.0011823
BDNF	1.8673435	0.0128883	C11orf54	-10.76763	0.002058
BPTF	1.5462241	0.0019616	C16orf89	-1.452363	0.0494525
BRD2	1.4977559	0.0045629	CACNA1G	-8.423466	0.0198543
C20orf194	10.355351	0.0046819	CALM3	-13.97925	0.0002197
CAPN15	2.1779751	0.0012614	CAST	-11.03617	4.36E-08
CCAR1	5.2918614	0.0103163	CBLB	-10.60424	5.88E-09
CCND1	1.3413465	0.0112397	CCDC144A	-8.791163	0.0023512
CCNT1	2.0455969	0.0160173	CCDC66	-7.370687	0.019206
CCPG1	10.37359	0.0122779	CCDC88A	-10.44432	0.0017084
CD164	2.5530094	0.0011296	CCND3	-10.54432	0.0046897
CD3EAP	1.7573318	0.0211451	CCPG1	-1.359124	0.0210363
CDC42EP3	1.2650313	0.0178822	CDH16	-4.343803	0.0494525

CDK12	1.2925343	0.0460089	CDH17	-1.540985	0.0087952
CDK6	3.0413408	0.0082926	CDK5RAP3	-12.07682	1.82E-06
CDKN1A	8.427662	0.0208231	CDKN1B	-1.526021	0.0040576
CENPO	2.9191689	0.0492223	CELF1	-7.279997	2.45E-09
CEP68	9.7976615	0.0311031	CHD4	-10.37359	0.0047605
CHD8	6.5534078	0.0067781	CIRBP	-11.28579	0.0120548
CHML	2.112099	3.72E-05	CKLF	-11.00609	2.19E-09
CHPF	10.116344	0.0055547	Cluh	-7.651052	0.0025188
CHST3	1.5050038	0.0123362	CNTNAP3B	-1.902422	6.10E-05
Cic	10.67948	0.0012072	COL12A1	-9.70275	0.021453
CKLF	10.92679	1.55E-08	CP	-2.22632	0.0348026
CLCF1	1.393981	0.0464753	CPLANE1	-8.544321	0.0490582
CLK2	1.7900485	0.0311031	CYGB	-3.162391	0.0096705
CNTRL	9.212699	0.0389477	CYLD	-10.57302	0.0012379
COA7	1.6799042	0.0030566	DAGLB	-11.02929	0.0275203
CPD	8.2447602	0.0082916	DDIT4	-1.32888	0.0018239
CPEB4	7.6677029	0.0378821	DDX17	-11.96338	0.0050554
CPS1	8.7813597	0.026222	DIDO1	-11.68241	6.18E-08
CPSF7	1.5201318	0.0063305	DOC2A	-10.63783	0.0033842
CRAMP1L	2.7288719	0.001527	DOK4	-11.00843	0.020141
CS	2.5729756	0.0100684	EHBP1	-11.99671	0.0002197
CSNK1G1	3.2103326	0.0102367	FAM167A	-11.0634	0.007698
CSNK1G3	10.778625	0.000203	FAM214B	-1.93138	0.0249503
CSRNP1	2.2087471	1.00E-05	FARSB	-10.5216	0.0275203
CSRNP2	9.0588937	0.0167722	FCGBP	-1.624808	0.0348257
CTGF	3.2686778	7.85E-17	FGD6	-1.533733	0.0291297
CTPS1	1.594844	0.0004246	FICD	-10.09891	0.0284439
CTSD	11.565102	0.0243355	FLNA	-1.122022	0.0269815
CUX1	4.3156418	0.0043884	FOXN2	-1.711249	0.0053392
CWC25	2.0814072	0.0250217	FRMD4B	-9.557145	0.0019616
CYR61	1.9019456	0.0006447	GGA3	-10.2127	0.0116806
DCAF1	3.5363936	0.0031049	GIGYF2	-10.58246	5.26E-05
DDB1	7.0768156	0.0066991	GOLGA4	-11.10547	0.0024692
DDX11	8.6677029	0.009229	GRB7	-9.803055	0.0279348
DDX3X	1.2394729	0.0418729	GVQW1	-10.63481	0.0167722
DDX5	1.1133573	0.0454875	H3F3B	-14.96909	5.29E-06
DENND1B	6.9541963	0.0001425	HOXB5	-1.563037	0.0257867
DIDO1	1.275745	0.0194421	ID1	-1.221078	0.0313653
DIO2	6.5616551	2.47E-06	ILF3	-10.94885	0.0229234
DKK1	1.7180897	0.0054163	INKA2	-9.137845	0.0029602
DLAT	9.9512847	0.0031049	INPP1	-12.11959	0.0011432
DMTF1	10.518325	0.0004386	IRF2BP2	-1.124534	0.0480236
DNAJB1	1.2773835	0.0115266	ISYNA1	-11.74539	3.90E-05
DNM1	10.936638	0.0119545	KATNBL1	-10.85331	0.0212913
DNTTIP2	1.8878829	0.0008097	KCNC4	-6.78136	0.0389477
DOCK10	9.0768156	0.0480236	KCTD7	-5.289507	0.0307637
DYNC1H1	2.0667578	2.50E-05	KIAA0232	-1.223616	0.0424385
DZIP1	8.6677029	0.0277956	KIAA1109	-8.936638	0.0421419
E2F6	2.0348928	0.0125069	KIF13B	-1.770438	0.0283755

EEF1D	2.5407197	0.0233929	KMT2E	-10.14211	0.0074641
EFNB2	2.4366734	0.0150881	KTN1	-8.906891	0.0438275
EFTUD2	9.212699	0.0262899	L1CAM	-9.67948	0.0014023
EGFR	8.5824556	0.0275722	LAMB3	-1.255727	0.037897
EGR1	2.2953088	0.0053361	LAMC2	-10.65284	0.0078668
EGR3	6.8454901	1.81E-06	LGALS9	-9.99906	0.0360186
EIF3C	1.7798556	0.0004465	LGALSL	-10.75377	3.39E-05
EIF4G1	10.291554	0.0026329	LGR6	-9.601152	0.0120632
EIF5	10.224806	7.09E-05	LIMS1	-10.90689	0.0344114
ELF4	10.86367	1.89E-06	LPCAT4	-3.336575	0.0005041
ELK4	8.0126245	0.0410349	LTBP2	-8.022368	0.000277
ENC1	3.0454241	4.45E-07	LTBP3	-1.281123	0.0348026
EPC1	1.7068411	0.0093348	MAMLD1	-10.04075	0.03077
EPC2	2.5902439	0.0008398	MAP1B	-13.00258	0.0001583
ERP29	12.585589	1.71E-08	MGA	-5.902878	0.0307637
ETS2	1.5179517	0.0018239	MIB1	-9.70275	0.0001094
F2RL1	1.3475527	0.0054163	MICAL1	-9.655829	0.0198543
FAM118A	10.501837	0.0006658	MPP5	-10.53138	5.54E-06
FAM133B	1.3478533	0.045299	MYH9	-10.835	0.0011432
FAM13B	2.0649697	0.0036602	N4BP2L2	-8.409391	0.0285354
FAM208B	1.5488932	0.0302113	NCOR2	-13.44648	1.50E-39
FAM222A	3.7504279	0.0041606	NDUFS2	-2.925999	0.0359574
FAM53C	1.9379813	1.05E-05	NFAT5	-1.312387	0.0406511
FGFR1	3.8303925	0.0332299	NKIRAS2	-11.77451	3.77E-05
FJX1	1.8694436	0.0093348	NLRX1	-10.24872	0.0436393
FLCN	1.6330085	0.0054899	NOL4L	-1.715076	0.0027063
FLNA	1.7342336	0.0050344	NOMO3	-11.95855	0.0004318
FNIP1	1.1460658	0.0402283	NR1H3	-10.23282	0.0310239
FOSB	3.9061618	0.0178052	NRF1	-11.15482	5.91E-06
FOSL1	1.7656423	0.0083512	NTRK3	-12.3526	9.94E-09
FOXJ3	2.0504533	0.0013152	NUDT12	-9.220781	0.0132622
FTSJ3	10.287712	0.0421419	NUMB	-2.587295	0.0452774
FUS	2.0397518	0.0490949	NUP98	-10.17159	0.0102514
GALNT10	1.5276702	0.0159254	OPRL1	-9.60733	0.0136979
GJA1	11.270295	0.0353752	OR1F12	-1.963058	0.0354208
GNPDA1	2.6155841	0.0307637	OTUD7A	-7.78136	0.0125069
GOLIM4	10.649855	0.0026567	PACSIN3	-11.76487	0.017437
GPR135	1.1890764	0.010396	PARP6	-12.31345	0.0064755
GREM1	3.6315629	0.0019838	PGM3	-11.48516	0.0198543
GRWD1	1.3174967	0.0135214	PHC2	-9.906891	0.0092518
GTF2I	9.8713919	0.0466566	PHF21A	-1.853611	0.0077291
GVQW1	4.0669502	3.70E-08	PHGDH	-10.77588	0.0047577
HACD2	11.32568	0.0025973	PIK3R1	-10.14636	0.0078157
HBEGF	2.0010892	0.0348026	PIM1	-2.062873	0.0002953
HELZ2	1.3242428	0.0275203	PLAU	-1.129859	0.0414895
HEXIM1	1.5844061	0.0041595	PLCL2	-9.260528	0.0383407
HMGCS1	1.7990964	0.0041595	PLD1	-1.635993	0.0378744
HMOX1	1.1594323	0.0450701	PLEC	-12.28675	1.29E-05
HNRNPA2B1	1.2813793	0.0112236	PLXNB2	-1.863693	0.0163911

HNRNPC	1.3070268	0.0210588	PPARA	-8.813781	0.0348371
HNRNPLL	10.384424	0.026439	PPARD	-8.965784	0.0475145
HSPA2	1.6549428	0.0036781	PRRC2C	-8.791163	7.55E-10
HSPA8	1.2251783	0.0257639	PTPDC1	-8.748193	0.0278428
IARS	2.3202157	0.000251	PUF60	-10.92432	0.0278451
IBA57	1.8932903	0.0389477	PUM2	-10.33688	0.0070256
ID2	1.2503617	0.0291297	QRICH1	-3.686303	0.0375052
IFFO2	1.4576112	0.0348257	RASGEF1A	-5.745954	0.0212913
IGF1R	11.177835	2.56E-05	RBL2	-10.69986	0.0212631
IL11	2.3051719	0.0096705	RBM33	-11.24674	0.0045808
ILF3	9.7085091	0.0166085	SAT1	-2.805283	4.15E-10
INTS2	7.693487	0.0126373	SCNN1A	-9.625709	0.0208391
IQGAP2	9.6073303	0.0369947	SCYL1	-1.710121	0.0115616
IRF7	2.0823778	0.0379365	SEMA4B	-1.368215	0.0084515
JMJD6	8.8559067	0.0125069	SEMA4C	-10.55075	5.44E-05
JUN	2.5471105	2.19E-09	SERPINA6	-10.43045	0.0256734
KANSL1	12.084587	1.03E-09	SESN1	-2.43385	0.0347955
KBTBD8	8.8968369	0.0178822	SETD1A	-9.736966	0.0260611
KCNAB2	5.9726927	0.0260611	SH3BP2	-2.405069	0.0109538
KCNQ5	8.212699	0.0349969	SHROOM3	-10.19229	3.18E-08
KDM6A	10.444325	0.0078668	SIX4	-5.193772	0.0347924
KLC1	2.6690268	0.0004465	SLC23A2	-2.06953	3.18E-08
KMT2C	8.129283	0.0378744	SLC25A29	-2.191951	0.0089973
KRT80	1.4115631	0.0125069	SLC25A39	-2.817168	0.0045808
KSR2	4.3865811	0.0152991	SLC7A2	-3.890402	0.0198987
LATS1	10.017736	0.0066884	SMARCA4	-9.50515	0.0025971
LATS2	1.9036423	7.36E-05	SNX5	-13.31864	0.0001064
LBH	1.8499705	0.0005041	SOD2	-1.378569	0.0347924
LIMCH1	8.821774	2.92E-17	SPRY1	-10.0634	0.045299
LMCD1	1.7911629	0.0466566	SRGAP2	-1.986203	0.0466566
LPCAT1	1.1006851	0.0487954	SYNE3	-8.619609	0.0215311
LRIF1	1.7632179	0.0086644	SYT17	-2.934112	0.0402283
LRRC58	1.2164386	0.0400812	TBC1D3L	-11.96458	1.48E-06
LYPLA1	11.523235	2.96E-06	TEP1	-9.74259	3.78E-05
MAFK	1.827625	1.68E-05	TGFB1I1	-11.29155	0.0391502
MALT1	3.020534	0.001211	TGIF1	-5.264623	0.0450701
MAP3K14	1.8359771	4.26E-05	TKT	-1.155679	0.0310237
MAPKAP1	10.582456	0.0198987	TMBIM6	-1.630056	0.0181374
MAPKBP1	1.8688773	0.0164677	TMCO4	-10.5411	0.000639
MARK3	10.081262	0.0132622	TMEM169	-9.731319	0.0113662
MBD5	8.6558288	0.0450701	TMEM219	-12.44519	0.007434
MDN1	1.9483158	0.0116927	TMEM265	-11.55395	0.0047251
MECP2	10.931722	9.11E-09	TMEM63B	-10.5216	0.0002114
MEF2D	4.1879252	0.0063305	TNFAIP2	-1.378607	0.0012057
MEPCE	1.4166581	0.0141755	TNFRSF10B	-1.292186	0.0249033
MGA	2.0896944	0.0077291	TROAP	-10.05438	0.0071909
MGAT5	10.260528	0.0042591	TTC39A	-9.931722	0.0210363
Mitf	10.491853	7.00E-06	TTC39C	-9.901873	0.0410349
MLLT10	9.7868141	0.0015227	UNKL	-10.39874	0.0005097

MMS22L	9.3143944	0.0216676	USP4	-9.886713	0.0089973
MRM2	2.4507299	0.0487954	UTY	-1.813781	0.0108394
MRPL27	2.1662188	0.0108394	VMP1	-2.225988	0.0020699
MRPS23	3.9490161	1.06E-06	VPS13A	-10.89178	0.0002984
MTCL1	1.3919988	0.0311031	WBP2	-12.10219	0.0071958
MTHFD1L	10.481799	0.0269815	WSB1	-1.950524	0.0005184
MT-ND6	1.0786568	0.0317723	ZBTB43	-9.994353	2.16E-05
MX1	2.9126438	0.0014018	ZDHHC7	-9.68825	0.0235054
MYC	2.2598307	0.0001064	ZMYND8	-10.37359	0.0256672
MYLK2	4.3846639	0.0485002	ZNF207	-9.582456	0.000583
NAB1	2.4704111	0.0439724	ZNF33A	-1.78736	0.0480236
NAB2	3.6326764	0.0003213	ZNF385A	-11.29539	0.0485002
NABP1	1.679728	5.44E-05	ZNF638	-11.17991	0.000583
NAV1	4.9954845	0.0291297	ZNF714	-2.431339	0.0233922
NCAPH	10.003752	0.0096705	ZSCAN2	-9.876517	0.0048573
NCL	1.8410192	0.0004318			
NCOA5	2.1432445	0.002208			
NCOR2	2.1480134	2.34E-05			
NFAT5	11.498517	5.59E-10			
NFRKB	9.3951771	0.0212631			
NHS	2.0012221	4.40E-05			
NIN	4.3434078	0.0249033			
NOMO1	8.8998604	2.48E-13			
NOMO2	10.840253	1.75E-05			
NOVA2	9.0588937	0.0022899			
NPEPPSL1	8.9753703	0.0291297			
NR4A1	2.6713502	2.45E-09			
NR4A3	5.7964666	4.56E-16			
NRP1	3.7839065	0.0449245			
NT5DC1	9.464886	0.0439299			
NUP98	2.0312138	0.0184785			
NVL	6.4195389	0.0101543			
OSGIN1	2.8317618	5.54E-06			
P2RY11	2.6206135	0.0040637			
PABPC4	1.9585172	0.0057253			
PAK4	1.6979913	0.0184785			
PANK1	9.9753703	0.0230925			
PARG	2.4293116	0.0006185			
PARP6	1.2344653	0.0427951			
PARVA	10.279997	0.0311031			
Pbx1	10.464886	0.0049052			
PCNX4	1.680667	0.0150518			
PDCD11	1.2551639	0.0275203			
PDE4D	1.6637885	0.049183			
PDXK	2.6589631	0.0307637			
PFKFB3	4.892504	0.0011296			
PFKP	2.0832165	0.0012621			
PIP5KL1	3.974909	0.0018378			
PLAGL1	9.9168747	6.22E-05			

PLK4	10.528128	0.0258607
PLOD2	1.3443676	0.0402283
PLXNA2	7.8662486	0.0106488
PMEPA1	2.3581817	0.0194421
PML	2.427454	0.0125069
POGZ	2.6420579	0.0206791
Pol	2.1355571	0.0001291
PPAN-P2RY11	3.0261128	0.0050344
PPP1R10	2.4827158	1.68E-07
PPP1R15A	1.3651061	0.0447683
PPP1R7	6.3477444	0.0081343
PPRC1	4.6776898	4.25E-07
PREX1	10.204571	0.0050554
PRICKLE2	1.6151559	0.0020699
PRKCE	11.12067	1.86E-10
PRRC2C	1.2292993	0.0269815
PSMD2	9.3365066	0.0052857
PTGS2	10.076816	0.0314913
PTPN3	5.6780719	0.0249503
PTPRA	5.3797722	0.0111853
Ptrf	1.3158723	0.019206
PTRH2	2.4028481	0.0100987
PVR	1.3136783	0.006535
QRICH1	1.7990513	0.0389477
QSER1	12.19332	0.0212913
RALGAPB	9.9848931	0.0398634
RAPGEF2	5.0195907	0.0349052
RARA	1.4586481	0.0448659
RBM12	2.1961205	0.0014018
RBM39	1.2003495	0.0421419
RBM6	2.6063679	0.0096066
RBPMS	9.7199592	0.0368251
RHOB	1.6110271	0.0064368
RND3	2.4450622	0.0014005
RNF41	9.6438562	0.0014018
RRP8	1.7619275	0.0050312
RTRAF	11.748193	0.0275203
SAMD4A	1.9107327	0.0013222
SCO2	8.0140205	0.0389477
SERTAD1	2.4845399	8.85E-06
SF3B1	3.0823224	4.58E-05
SFPQ	1.4143226	0.0338318
SGK1	2.4961682	5.11E-05
SHANK3	9.6196086	0.0030519
SHROOM3	10.531381	0.0007393
SIM2	1.512313	0.0135827
SIN3A	9.6438562	0.023802
SKIL	2.0183785	0.0015166
SLC12A4	8.8968369	0.045299

SLC2A3	1.4075372	0.0120632
SLC30A1	1.4319401	0.0047605
SLC30A9	9.4374053	0.0012176
SLC38A1	9.3516754	0.0466566
SLC43A1	9.5313815	0.0495486
SLC7A6	2.2859555	0.0002327
Smad7	2.5867038	0.0132622
SMARCA4	9.0945176	0.0070256
Smc1a	8.8662486	0.0003196
SMCR8	1.221291	0.0160385
SMG1	8.792248	0.0071958
SMIM15	11.039605	4.71E-14
SMN1	11.426964	0.007916
SNAI2	2.8519617	0.0037647
SNRNP200	12.067882	1.05E-18
SOX4	1.2709053	0.0088081
SPATA6	8.8349977	0.025563
SRCAP	1.5308668	0.020555
SREK1	1.8916692	0.020555
SRGAP3	8.9168747	0.0450847
SRRM2	1.4683777	0.0379092
SRSF1	2.0059144	0.0009579
SRSF4	1.4592857	0.0269815
SRSF6	2.9166003	4.55E-05
SRSF7	2.2421318	9.80E-05
SRXN1	1.2790644	0.0212913
STAG2	9.137845	0.0086644
STC2	2.0838606	0.0125069
STK10	8.8030548	0.0104796
STON2	9.9366379	0.0030519
SUPT6H	1.840872	0.0030519
SYDE2	1.9702165	0.0353752
SYNM	1.8323947	0.0001291
SYPL1	5.89458	0.0007102
TBL1XR1	8.1649069	0.0377858
TBX3	2.1311449	5.54E-06
TCF4	8.9366379	0.0368005
TDG	11.978949	5.33E-09
TENT5A	10.423466	0.0133355
TGFB1I1	12.262486	1.51E-07
TGFBI	1.879129	0.0110704
THBS1	3.1073533	0.0004383
TLE4	4.582308	0.0495486
Tlk2	7.4076926	0.0178052
TMEM219	12.779309	4.16E-06
TNFRSF12A	2.5241946	0.0064897
TNS3	12.302068	4.69E-05
TNS4	2.0699603	5.35E-05
TP53I11	11.563514	6.03E-07

TRAPPC10	8.8867127	0.0027063
TRAPPC11	9.9366379	0.04859
TRAPPC9	10.550747	0.0262734
TRIM21	1.2773349	0.0494525
TRIM25	1.1126244	0.0353752
TRNT1	10.86367	0.0011267
TSC22D2	2.1163542	0.0001064
TSPAN14	2.1630509	2.20E-06
TUFT1	3.3201459	1.55E-08
UBAP2L	10.708509	0.0049239
UPF3B	10.026984	0.0113865
URB2	1.4718497	0.0127937
USP36	1.2306541	0.0480236
USP38	2.0116818	0.0275203
UTY	1.6309854	0.035919
VGLL3	8.464886	0.0019366
VPS53	1.63768	0.0430756
WDR1	11.898097	1.59E-09
WDR3	1.9265902	0.0379092
WDR41	8.7703886	0.0495486
WDR43	1.3122017	0.0246224
WIZ	5.4550532	4.25E-07
WWP2	10.739781	0.0435037
WWTR1	10.585589	0.0028325
XPO4	8.7027499	0.0406511
XRCC2	9.5443205	0.0003864
ZBTB37	2.4966357	0.017101
ZC3HAV1	2.3432656	2.37E-09
ZFPM1	2.1269121	0.0480236
ZFY	10.511753	5.83E-06
ZNF10	8.8867127	0.019206
ZNF227	11.169507	6.41E-06
ZNF280C	10.179909	0.0002197
ZNF283	8.4374053	0.0163911
ZNF331	2.3174571	0.0002984
ZNF35	3.1063383	0.0378744
ZNF426	8.4784326	0.0151786
ZNF451	1.8789082	0.0007479
ZNF469	2.5889644	4.77E-06
ZNF480	10.146357	0.0006246
ZNF714	1.560152	0.0378744
ZNF805	8.7481929	0.0308477
ZSCAN25	10.731319	5.83E-06

Table S7. Different expression genes(DEGs) in NR0B1 KD cells

up-regulated DEGs	log2(FC)	FDR	down-regulated DEGs	log2(FC)	FDR
ABCA1	1.6633554	0.0471534	ABCC8	-6.98868	0.0481039
ABCC5	1.6884063	0.0384787	ADCK4	-11.28386	2.07E-05
ABCG1	7.7515441	0.0022526	ADGRL2	-10.14211	0.0001315
ACLY	2.4572195	0.0010134	ADM	-2.25646	0.0005596
ACO1	11.675075	5.29E-09	AFAP1	-1.58841	0.0044531
ACSL3	11.355351	0.0305418	AHR	-2.15710	2.69E-05
ACTN4	1.4965102	0.018092	AJUBA	-2.25704	2.29E-06
ADAM19	2.3318549	1.58E-08	AKNA	-4.00000	0.0470276
ADAMTS15	8.9657843	0.0023738	ALKBH3	-2.68885	0.0192165
ADAMTS7	2.697172	0.0088252	AMOTL2	-1.68558	0.0027348
ADCY1	8.5824556	0.022853	ANKRD1	-4.28736	1.36E-06
AKAP1	1.8531227	0.0112246	ANKRD33B	-1.20652	0.0441217
AKR1C2	2.1822664	0.0010134	ANKRD40	-1.96871	0.0150368
ANKFY1	9.4580648	0.0244277	ARHGEF18	-10.72849	0.0002264
ANO10	9.7369656	0.0262467	ARMT1	-9.22078	0.0470276
APC	10.179909	0.0016594	ARRB2	-1.55487	0.047478
APOL1	3.5897635	0.0003856	ARRDC4	-2.97147	0.0351475
APOOL	9.8559067	0.0105534	ARX	-4.64725	0.0139563
ARHGEF10	8.8968369	0.0083916	ASNS	-1.59858	0.0038688
ARHGEF4	3.8712667	0.0492625	ASPH	-1.59895	0.0059896
ARL4C	1.4100736	0.0160643	ATF3	-2.86031	4.67E-06
ASS1	2.109987	0.0274854	ATOH8	-2.43324	0.0340705
AXIN2	2.6287736	0.0309527	ATP11C	-10.63178	0.0025161
BAAT	1.8115093	0.0402734	ATXN2	-1.81523	0.0238066
BAHCC1	10.553949	4.26E-11	BAG6	-12.18405	2.12E-16
BBS2	9.9561341	0.0066587	BAZ2B	-7.93664	1.35E-05
BCL2L11	1.9616299	0.0098439	BBS10	-9.53138	0.0044531
BEAN1	2.8124348	0.0052242	BCAT1	-1.91433	0.0040756
BLMH	12.701306	5.51E-13	BMF	-8.77039	0.0149935
BMF	11.695518	2.15E-08	BZW2	-2.89891	0.0152373
BMP1	1.4003561	0.0248372	C19orf25	-10.05438	0.0093683
BOK	9.0223678	0.0001163	C2CD2	-9.43741	0.0284906
BRMS1L	11.694068	6.95E-08	CARS	-1.45503	0.0316948
C1R	3.1716585	0.0354875	CBS	-1.43487	0.0404306
C1S	10.655829	0.0007013	CCDC144A	-9.53138	0.031804
C3	1.8139548	0.0028847	CCDC88C	-9.10329	0.0351475
CALM3	12.037318	0.0110852	CDC42EP1	-1.65886	0.0009404
CARD11	10.098909	3.36E-05	CDKN2AIP	-2.00757	0.0290116
CAST	10.232821	0.0310945	CEACAM6	-1.73092	0.0059896
Cbx1	12.318166	0.0040385	CENPK	-10.32942	0.0261335
CCBL2	10.946419	0.0003264	CEP44	-9.23681	0.0052118
CCNG1	13.113091	0.0085254	CHD4	-9.63178	0.0164593
CDC42BPG	9.5507468	0.0263303	CHIC1	-1.85062	0.0496104
CDH6	9.9218409	0.0037987	Cic	-9.72565	0.006487
CDK12	9.7085091	1.41E-07	CIZ1	-11.73273	7.62E-09
CFB	4.2371073	0.0139826	CLASP1	-8.42347	0.0227622
CHTF8	11.712814	0.0044531	CLBA1	-10.32942	0.0178552

CLDN2	1.7040551	0.0021707	CLDN1	-2.05943	5.41E-05
CNP	1.7931853	0.0004524	CLIP1	-8.87652	0.0209754
CNTNAP3B	11.32568	0.006505	CNKSR2	-7.92679	0.0460815
COBLL1	7.3219281	0.0471534	CNKSR3	-1.59841	0.0479658
COL1A1	2.0577835	0.0082874	CNOT6	-11.11634	6.40E-13
COL22A1	8.9848931	0.0050269	CPEB4	-1.65436	0.0132205
Col24a1	5.4607426	0.0092684	CREB5	-1.88670	0.0056236
COL4A1	1.2212988	0.0280627	CTGF	-1.65090	0.0032447
COL5A1	2.2323898	3.36E-05	CTNND1	-9.58246	0.0344413
COL6A2	1.662394	0.042937	CTPS1	-1.62976	0.0088252
COQ2	12.447772	0.002828	CYR61	-2.72711	1.35E-07
CSE1L	12.485158	1.14E-10	DAGLB	-1.42701	0.028205
CTIF	8.8559067	0.0128484	DLC1	-2.76407	3.98E-07
CTSB	9.5824556	0.0059571	DNAH17	-7.90689	0.0009947
CYB5RL	8.212699	0.030621	DNAJA3	-1.52710	0.0252084
DCLK2	8.9366379	0.0411005	DOCK11	-9.22882	0.0018767
DIDO1	9.8030548	0.0081633	DUS2	-9.70851	0.0474584
DLGAP5	9.5761694	0.0074199	DUSP1	-1.57707	0.0032971
DNAH17	9.0223678	3.91E-06	DUSP8	-10.09891	0.0188638
DNAJA1	1.4651894	0.0197691	EHMT2	-9.74819	0.0486046
DNAJC21	9.5183253	0.0494054	EIF3A	-1.37275	0.0471534
DNMT3A	9.2207814	0.0141039	ELAC2	-10.88162	0.0134605
DOCK10	9.4443247	0.0184326	EML4	-1.77620	4.78E-05
DOCK7	9.6134825	2.34E-05	EPB41L2	-9.81911	0.003354
DPYSL5	2.2232655	0.0351475	ERCC1	-11.86754	0.0147738
ECE1	9.7703886	0.0248388	ETNK1	-1.50386	0.0174126
EEF1A2	10.285402	0.0036258	ETS1	-1.65412	0.0105303
EGFR	11.924318	2.15E-08	FAM129A	-1.74561	0.0033031
EIF2S1	11.065641	0.0033871	FGF2	-1.80843	0.0025161
EIF3A	12.388914	6.50E-08	FLNB	-14.82658	3.20E-79
EPHB2	1.2287227	0.0449721	FOSL1	-1.86733	0.0162543
ERVK-6	7.4374053	0.0496395	FRMD3	-3.10404	3.23E-09
EZH1	9.8137812	0.0088252	FRMD6	-1.43957	0.0373564
FAT1	1.3817755	0.0486046	FUT1	-8.69116	0.0402734
FBH1	9.1715938	0.0115923	GADD45A	-2.20581	1.35E-05
FBXO18	9.2045711	0.0149935	GADD45B	-2.38047	0.000501
FBXO6	10.501837	0.0121119	GARS	-1.25197	0.0201544
FLNC	9.112005	4.31E-05	GFRA1	-2.28011	0.0003781
FLOT2	1.2848053	0.0434748	GGT1	-10.17159	0.0143256
FMN1	8.5313815	9.22E-05	GOT1	-1.83036	0.0005574
FRMD4A	9.4443247	0.034663	GPRC5A	-1.82700	0.0008562
FSTL1	1.9700214	1.25E-05	GRIK2	-8.79225	0.014684
FSTL4	2.8073549	0.0032971	GSE1	-3.95977	0.031804
FZD5	1.3056318	0.0470746	HECTD1	-11.09011	1.17E-15
GALNT12	2.1577447	0.0464552	HERC2	-7.64386	0.0429911
GIT2	9.4234661	0.0018767	HIPK3	-11.15693	1.38E-15
GLIPR1	1.7279205	0.0395099	HIVEP2	-2.69883	0.0039419
GNE	9.1206699	0.004982	HKDC1	-1.55847	0.0006245
GNG2	2.7129487	0.0448874	HNRNPUL1	-11.83091	1.13E-29

GOLGA1	7.9848931	0.0022526	HTR1D	-10.72565	0.00031
GOLGA4	11.648358	0.0001016	IDE	-10.86882	0.0016339
GOLGA8O	6.9503129	0.0242188	IGF2R	-7.92679	0.0009255
GRAMD1A	2.0765957	0.031804	IKBKB	-9.02237	0.023112
GRAMD1B	5.6475745	0.0085254	IKZF4	-8.92679	0.0059896
GRB10	9.5183253	0.043713	ITPRIPL2	-10.78136	0.0011578
GVQW1	3.560715	0.0021773	JUN	-1.26058	0.017777
HAS2	3.1474483	0.0050375	KDSR	-11.43914	0.0008562
HERC1	8.6438562	0.0101999	KIAA0226	-9.21270	0.0318564
HIVEP2	9.7369656	1.57E-06	KIF1A	-9.25267	0.0027498
HMGCS1	10.30302	0.0373155	KMT2C	-7.84549	0.0010134
HNRNPA1	11.85331	0.022853	KMT2E	-9.50515	0.031393
HPGD	1.288846	0.0115923	KRT80	-2.53347	3.91E-08
HSPA12A	1.6424594	0.0013995	KTN1	-12.23282	2.77E-19
HSPA1A	3.4288352	6.26E-05	LARS	-12.70923	3.45E-05
HSPA1B	2.8612827	0.0022487	LCORL	-8.43741	0.0448874
HSPA8	3.1834512	7.42E-06	LGALSL	-8.88671	0.0205215
HSPB1	1.4477838	0.0044995	LHX8	-3.52874	0.0416783
IFI27	8.2455527	0.0390166	LIMCH1	-3.87177	0.014684
IFI44	5.4326181	0.0197603	LITAF	-1.51720	0.0081633
IFI44L	8.3264295	0.0480585	LRPAP1	-9.97537	0.0120643
IFI6	6.9233042	0.0055877	LTBP3	-5.48583	0.0383706
IFIT1	6.1325336	0.0036352	MALL	-11.69986	0.0055851
IFIT3	4.2345057	0.0439942	MAP1LC3B	-1.51962	0.0036352
IFITM3	4.9581018	0.0127653	MAPT	-8.05889	0.0494054
IGFBP7	2.0639001	0.0002247	MARS	-1.37164	0.0100275
IL6ST	8.1963972	0.0042661	MEF2D	-1.57340	0.0085275
IQCE	9.3808218	0.0464638	MFF	-11.38262	0.0009255
IRF7	12.144233	3.66E-05	MFI2	-12.59805	0.0009034
ISG15	5.3885605	0.0060563	MIA2	-1.70701	0.0093578
ITGA11	9.0588937	0.0001056	MID1IP1	-8.95613	6.38E-10
ITSN1	10.550747	0.0393035	MIER1	-3.28831	0.0086628
KANK2	10.41996	1.35E-05	MITF	-1.54888	0.0197691
KCNJ6	2.0619277	0.0470276	MKI67	-1.93959	0.017722
KCNMA1	3.2822139	0.0001608	MMAA	-8.46489	0.0045279
KDELC2	1.7789209	0.0203916	MTSS1L	-1.70034	0.0031789
KLHL5	10.295386	0.0002126	MVP	-11.87907	0.0037987
KREMEN1	10.544321	0.0022044	MYADM	-2.84075	0.0281643
KRT19	1.4039763	0.0193973	MYC	-1.45153	0.0188638
L1RE1	1.9488273	0.0087121	MYH9	-11.89178	6.89E-05
LGALS3BP	2.3650076	0.0266593	NARS	-2.63923	0.0383706
LHFPL2	11.676545	0.000549	NEDD9	-2.40823	0.0440651
LIMS1	2.1121288	0.0107217	NFAT5	-10.24079	1.12E-06
LINGO1	9.1632303	0.0150368	NFE2L2	-1.27754	0.0416783
LIPH	9.0223678	0.0278662	NFIB	-1.42014	0.0109541
LLGL2	10.524868	0.0192165	NFIC	-11.86496	1.92E-06
LPCAT1	1.849071	0.018092	NOP2	-1.56844	0.0141035
LPIN2	11.063395	0.0006447	NOP56	-13.25267	7.39E-17
LRP1	1.6759999	0.0019873	NTNG2	-9.51833	3.01E-06

LRRC4B	9.7199592	0.0087121	NUAK2	-1.29280	0.0129483
LRRN2	9.9218409	0.0009404	PAWR	-1.20060	0.0227174
LTBP2	1.929791	0.0016284	PCLO	-2.11905	0.0243026
LTBP3	7.1996723	0.004191	PDE3A	-3.32278	1.00E-06
MAGED1	1.4942177	0.023112	PDE5A	-8.42347	0.00541
MAP2K5	10.103288	0.0193973	PFAS	-9.17159	0.0048169
MAPKAPK3	11.369961	1.12E-06	PHLDB2	-11.74679	1.79E-16
MAPRE2	9.9218409	0.0336268	PIP5K1A	-1.53589	0.0025451
MAST4	8.4918531	0.0096077	PLCXD3	-8.60733	0.0038994
MEGF8	1.9530757	6.46E-05	PPFIBP2	-2.30168	8.28E-05
MEGF9	1.4750196	0.0263303	PPM1B	-1.33129	0.0462937
MGRN1	10.409391	0.0033871	PPP1R15A	-2.47944	1.10E-07
MIB2	9.7142455	0.0032126	PRKAG2	-2.60720	0.0056294
MLH3	10.01309	1.00E-06	PRKCG	-9.01309	0.0488502
MPRIP	11.807087	2.87E-05	PRKCH	-6.32193	0.0023738
MT1F	2.4099769	0.023112	PTP4A1	-1.18813	0.0308522
MT1X	2.4977913	0.0027065	PVR	-1.29875	0.0128351
MT2A	1.4432246	0.0278944	PXDC1	-10.23681	0.0278762
MX1	9.3341935	0.0008562	QSER1	-9.64985	0.0231688
MYD88	1.745821	0.030828	RAB39B	-3.72367	1.05E-06
MYH10	1.495049	0.0344413	RCAN1	-2.01037	0.0015842
MYL6	1.7733149	0.0055877	RND3	-1.64021	0.0010588
MYLK	2.3345557	0.0172238	RPS2	-3.79510	8.21E-06
NAV1	2.8909283	0.0022339	RPS6KC1	-9.31439	0.0068068
NCOA4	1.7367433	0.0446901	RSF1	-9.09452	0.0091414
NID1	2.5611051	0.0001412	RSL1D1	-1.32718	0.0263303
NKD1	4.2065622	6.40E-13	RUSC2	-1.36767	0.0036258
NOTCH3	2.2727659	0.00023	SAMD4A	-1.81222	0.0147241
NPTX1	2.5507985	3.42E-06	SARG	-8.04075	0.0492085
NPTXR	1.4944974	0.0231688	SEC31A	-11.34614	1.67E-07
NSD2	9.3068212	3.30E-05	SERTAD2	-1.28396	0.029542
NT5E	1.6503201	0.0038688	SESN3	-1.80215	0.0203916
NVL	4.8181617	0.0405115	SETD5	-1.35653	0.0460815
OAS1	5.12747	0.0344413	SIRT7	-8.39518	0.0126829
OAS2	9.9815673	0.0017993	SLC16A7	-2.00405	0.0009113
OAS3	3.1235106	0.014844	SLC1A3	-11.34245	1.14E-10
OGT	13.156399	3.67E-33	SLC1A4	-1.72593	0.0231292
OLFML2A	1.5821747	0.0404306	SLC38A1	-1.29166	0.0351475
OLFML3	3.0611894	0.0021929	SLC38A10	-10.90689	0.0273638
PARP9	3.169925	0.0280627	SLC38A2	-1.62845	0.0445297
PCF11	10.433933	0.0019873	SLC6A15	-2.37676	0.013522
PCMTD1	10.824428	3.52E-06	SLC7A2	-10.27612	0.003011
PCNA	1.2877271	0.0075894	SMAD3	-11.15903	0.0240636
PEX26	8.9848931	0.0059571	SMARCA4	-8.96578	0.0114284
PHF19	9.4851584	0.0073381	SMG9	-1.56336	0.0197691
PHKA1	11.07904	4.22E-09	SNAPC1	-1.81747	0.0019652
PIK3CA	7.9848931	0.0091756	SNTB1	-1.93847	0.0389914
PITPNM1	9.6558288	0.001453	SNX10	-9.66178	0.0257073
PLEC	1.4087424	0.0126153	SPX	-2.09910	0.0283624

PLEKHA6	2.8210299	0.0099546	SRGAP2	-7.65821	0.0295141
PLEKHG5	9.5571446	0.0085254	Srsf3	-1.90009	0.0004914
PLXNA2	9.989631	0.0092978	SSRP1	-11.28000	0.0141039
PLXND1	1.832487	0.0019542	STC2	-2.22734	4.23E-06
PMEPA1	3.0617477	4.17E-07	STK32C	-9.72565	0.0448874
PML	2.6482191	0.0263303	SVEP1	-3.84410	7.56E-05
PODXL	2.1974807	9.64E-07	SYBU	-6.00817	0.0019873
POLE3	12.41996	2.15E-08	SYNE1	-1.31652	0.0182762
PPARA	8.4234661	0.0480585	SYNRG	-10.34799	4.22E-09
PPP1CB	9.9705853	0.0359289	TAX1BP1	-10.03159	0.0010134
PSMD2	10.824428	0.0205519	TBL1XR1	-9.30682	0.0141039
PTPRN	9.6011517	0.0033329	TCEA1	-1.18982	0.0470276
RAB15	10.821774	0.0098439	TESK1	-11.20661	0.0121437
RABL6	9.0037521	0.0464638	TFE3	-1.28190	0.0494054
RASA4	9.9801396	2.69E-05	TGIF1	-12.76763	0.000697
RASSF10	2.0886777	0.0020424	TMEM144	-9.11201	0.0227174
RASSF5	9.3663222	0.0108896	TNRC6C	-8.46489	0.0012788
RGS11	9.5887146	0.0288185	TRIB3	-2.16316	0.0001608
RGS3	9.3735902	0.0434748	TSC22D3	-1.67471	0.0315468
RIDA	11.010761	0.0318008	TUFT1	-1.40768	0.0110038
RNFT2	11.421714	0.0104372	TUSC3	-12.09121	1.37E-05
RPS3A	2.0365033	0.0184711	TXNIP	-2.86507	0.0460815
RPS9	12.218765	0.0315065	UBTD2	-11.56510	0.0035664
RPUSD1	9.8030548	0.0251114	USP1	-10.16742	0.0388375
RRBP1	2.8629927	0.0197691	USP53	-1.59353	0.0194335
RSPO3	1.2924993	0.0383706	VGLL3	-8.43741	0.0013063
RTN4RL1	2.5364557	0.0086628	WDR1	-3.99906	0.0182089
S1PR3	1.4120651	0.0149935	XPOT	-1.25625	0.0284906
SBNO2	9.5635141	0.0016594	ZC3H11A	-3.78840	0.022853
SDC1	1.3712414	0.00541	ZNF18	-10.13785	0.0252084
SEMA4D	10.040746	0.0423868	ZNF331	-10.09011	0.0121119
SERPINE2	1.3393212	0.0344413	ZNF460	-1.35999	0.0101999
SHROOM3	9.129283	0.0149935	ZNF772	-8.71425	0.0092684
SIPA1L1	7.5698556	0.0473576	ZSWIM8	-5.04439	0.0495645
SIRT7	8.2288187	0.0172326			
SLC16A3	2.0526611	0.0070337			
SLC25A22	10.30302	0.0492328			
SLC2A14	6.4178525	0.0101999			
SMARCE1	1.5518196	0.0363708			
SNRPA1	11.602699	0.0054966			
SORCS2	3.1557947	0.0131471			
SPECC1	1.3418349	0.03219			
SPINK13	11.085694	0.0165066			
SPOCK1	2.0767572	0.0016337			
SPP1	1.274402	0.011326			
SRSF1	1.5290243	0.0460815			
STARD8	9.8816238	0.0229337			
STC1	2.5400273	0.0035664			
STRIP2	2.3003949	0.0405849			

SYT13	2.9902917	8.07E-14
TAGLN	1.9521892	0.0090975
TARBP1	1.8439084	0.0068763
TGFBI	14.713351	1.49E-21
TGFBR1	2.2254855	6.57E-05
TGM2	1.3150365	0.0368041
THBD	2.1119684	0.0014902
THOC2	9.8137812	0.0056013
TIAM2	9.1799091	0.0051523
TLK2	9.5051499	0.0096077
TM4SF18	11.591834	0.0012488
TMEM120A	11.382624	0.0036258
TMEM63B	8.9168747	0.0450565
TMSB4X	1.1423525	0.0445585
TNC	2.3577981	0.0320711
TNFSF10	11.658807	0.0203916
TNS1	2.3488951	0.0023738
TNS4	1.374694	0.0039419
TP53I3	1.2965212	0.0496104
TP53INP1	1.9820983	0.0043674
TRAK1	10.216746	0.0105303
TREX1	11.692616	0.0134605
TRIM24	1.2738813	0.0383706
TSPAN14	1.48951	0.0167166
TSPAN18	1.8977389	0.0418273
TTC3	1.6224859	0.004191
TTYH3	1.3234371	0.0189582
TUBB4B	1.3989374	0.0239691
UBE2V1	12.68825	0.0009849
UBN2	5.5647846	0.0471534
VANGL1	1.4171764	0.0399939
VCAN	1.4139603	0.0032971
WWP2	9.8713919	0.0446365
XDH	2.3533233	0.0308522
ZC3HAV1	2.5912351	1.35E-07
ZMAT3	1.8898629	0.0009517
ZNF184	9.5507468	0.0076722
ZNF678	8.3663222	0.0050269

Table S8. Enriched ferroptosis-related genes in NR0B1-KD cells

Symbol	Description	Function
ATF3	Activating transcription factor 3	Inhibit SLC7A11 expression
GOT1	Glutamic-oxaloacetic transaminase 1	Increase αKG production
CBS	Cystathionine beta-synthase	Convert homocysteine to cystathionine
SLC38A1	Solute carrier family 38 member 1	Increase L-glutamine uptake
NRF2	Nuclear factor, erythroid 2-like 2	Induce antioxidant gene expression
c-JUN	Jun proto-oncogene, AP-1 transcription factor subunit	Induce transcription of CBS
AKR1C2	Aldo-keto reductase family 1 member C2	Catalyze NADPH-dependent reductions
NCOA4	Nuclear receptor coactivator 4	Mediate ferritinophagy
HSPB1	Heat shock protein family B (small) member 1	Inhibit iron uptake

Table S9. Enriched ferroptosis-related genes in NR0B1-OE cells

Symbol	Description	Function
SAT1	Spermidine/spermine N1-acetyltransferase 1	Increase ALOX15 expression
CS	Citrate synthase	Increase mitochondrial fatty acid metabolism
c-JUN	Jun proto-oncogene, AP-1 transcription factor subunit	Induce transcription of CBS
HMOX1	Heme oxygenase 1	Mediate heme catabolism

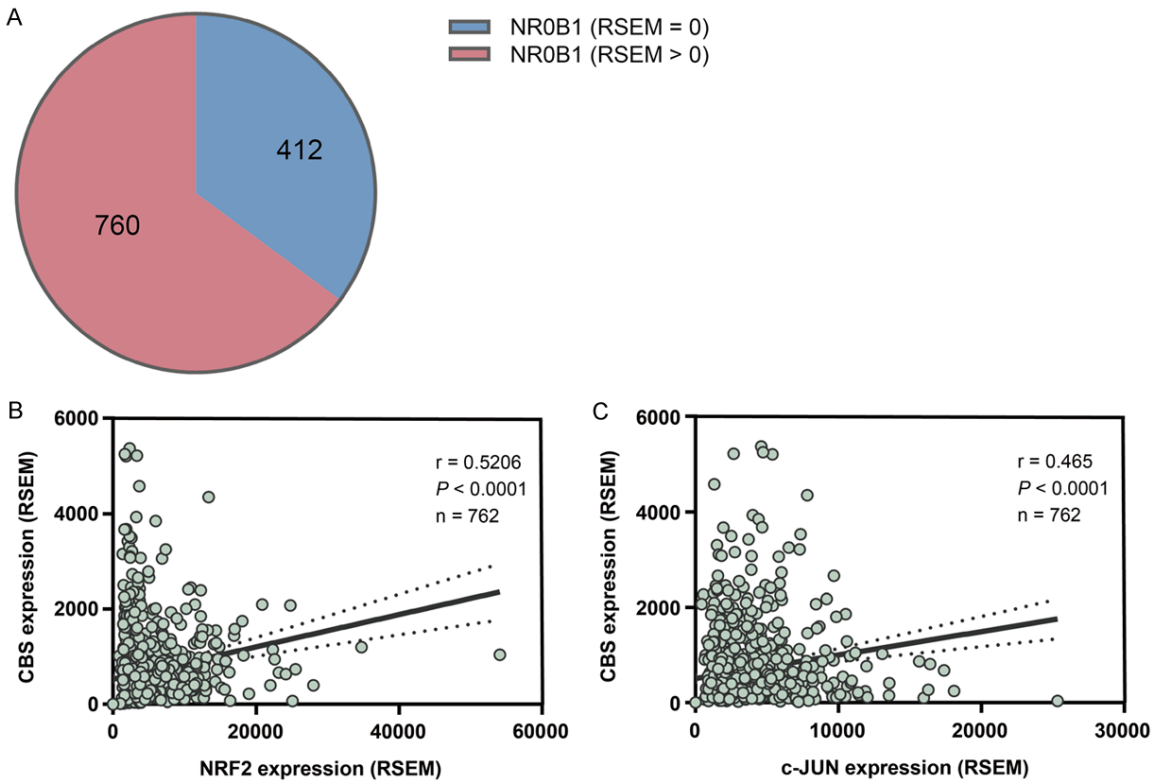

Figure S3. Ectopic expression of NR0B1 in lung cancers and correlation analysis between the expression of *CBS* and that of *NRF2*, *c-JUN*. (A) NR0B1 is activated in 760 out of 1172 lung cancers (RSEM > 0). (B, C) The *CBS* expression level was positively correlated with that of *NRF2* (B) and *c-JUN* (C).

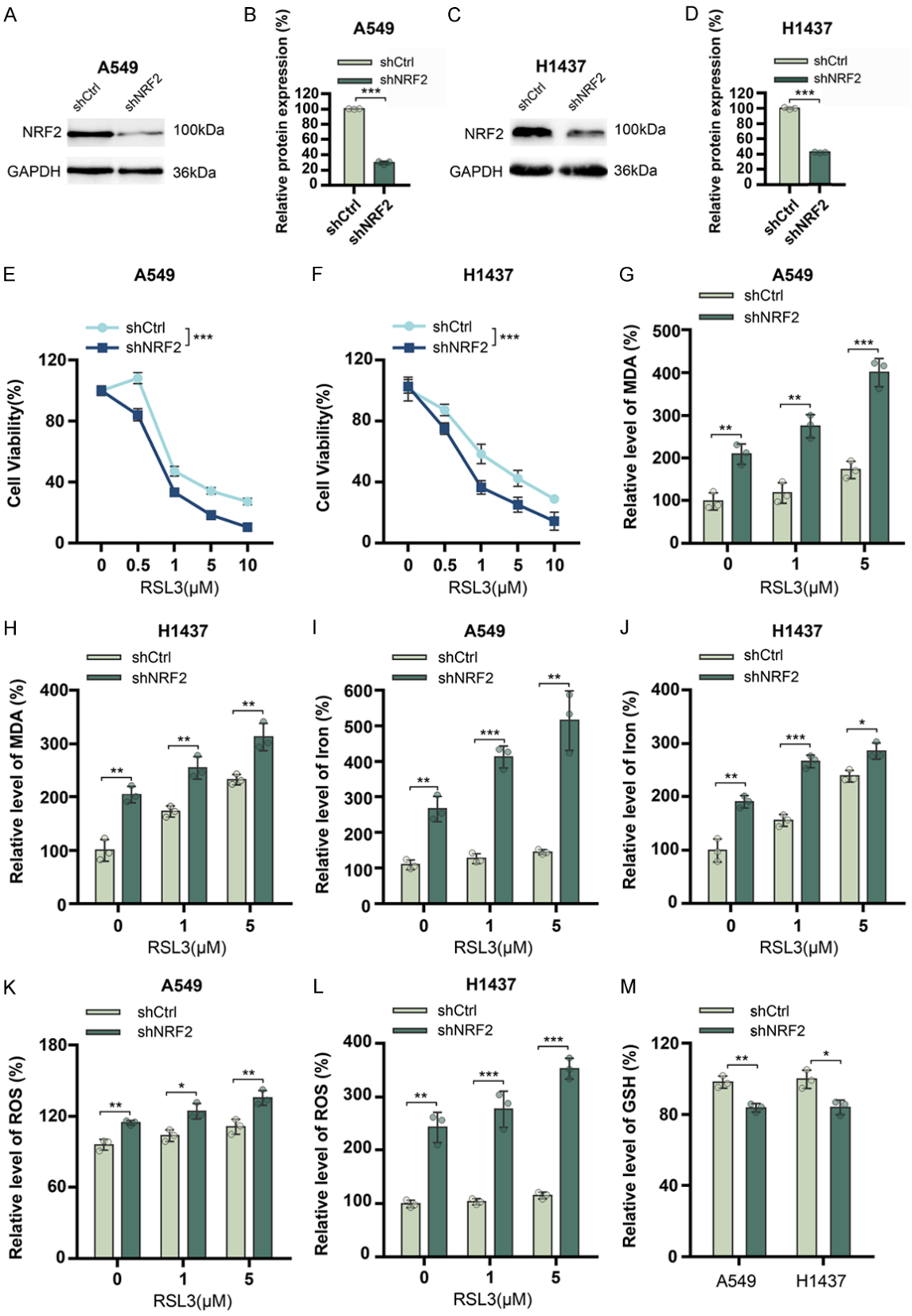

Figure S4. NRF2 knockdown enhances ferroptosis in lung cancer cells. (A, B) The protein expression level of NRF2 was decreased in NRF2-KD A549 cells. (C, D) The protein expression level of NRF2 was decreased in NRF2-KD H1437 cells. (E, F) Cell viabilities of A549 (E) and H1437 (F) under the treatment with different concentrations of RSL3 (0, 0.5, 1, 5, 10 μM). (G, H) Relative MDA levels in the lung cancer cells of A549 (G) and H1437 (H) under the treatment with different concentrations of RSL3 (0, 1, 5 μM). (I, J) Relative iron levels in the cells of A549 (I) and

H1437 (J) treated with RSL3. (K, L) Relative ROS levels in the cells of A549 (K) and H1437 (L) treated with RSL3. (M) Relative GSH levels in the lung cancer cells treated with RSL3. Data are presented as mean ± SD, $*P < 0.05$, $**P < 0.01$, $***P < 0.001$.

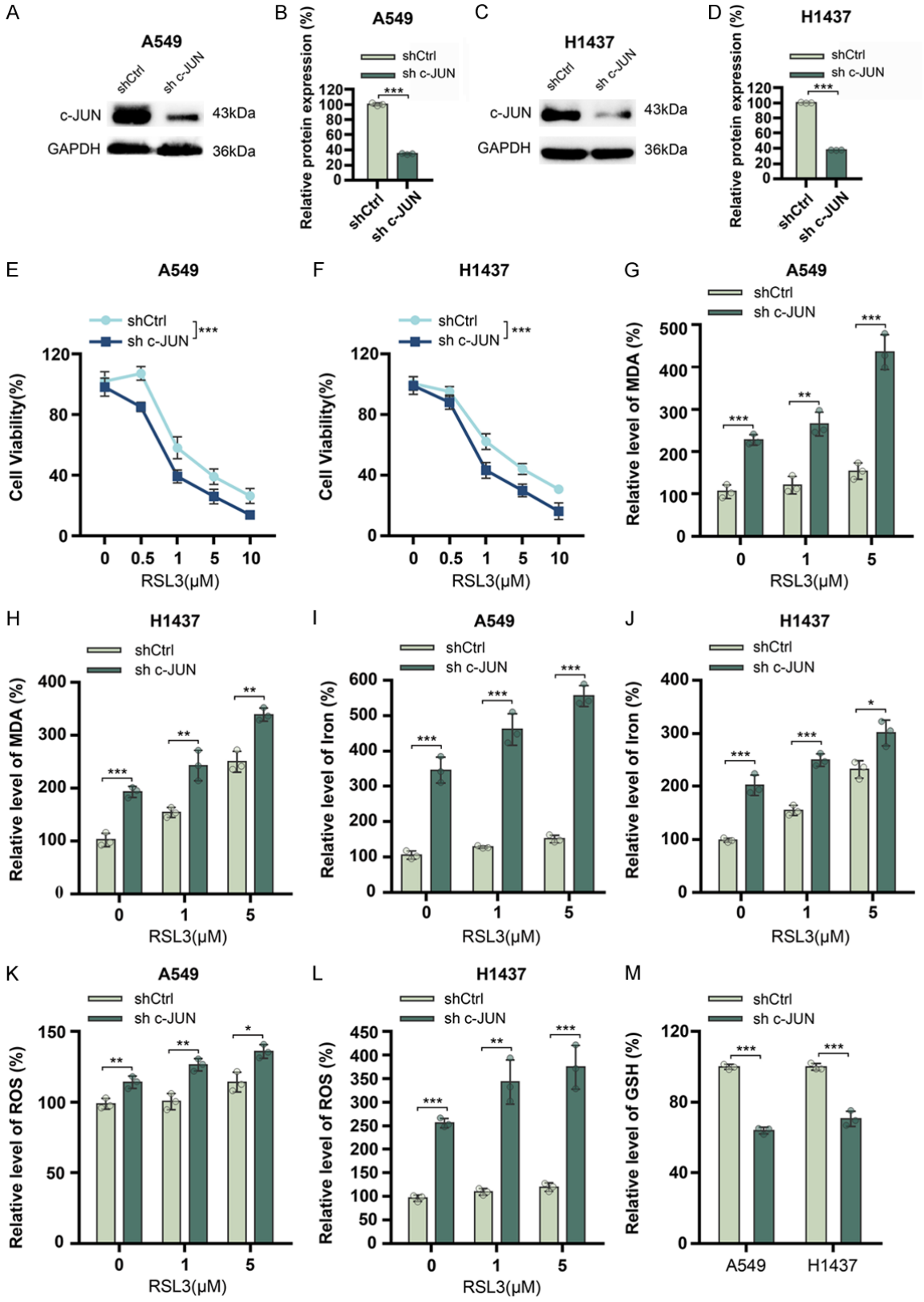

Figure S5. c-JUN knockdown enhances ferroptosis in lung cancer cells. (A, B) The protein expression level of c-JUN was decreased in c-JUN-KD A549 cells. (C, D) The protein expression level of c-JUN was decreased in c-JUN-KD H1437 cells. (E, F) Cell viabilities of A549 (E) and H1437 (F) under the treatment with different concentrations of RSL3 (0, 0.5, 1, 5, 10 μM). (G, H) Relative MDA levels in the lung cancer cells of A549 (G) and H1437 (H) under the treatment with different concentrations of RSL3 (0, 1, 5 μM). (I, J) Relative iron levels in the cells of A549 (I) and H1437 (J) treated with RSL3. (K, L) Relative ROS levels in the cells of A549 (K) and H1437 (L) treated with RSL3. (M) Relative GSH levels in the lung cancer cells treated with RSL3. Data are presented as mean ± SD, $*P < 0.05$, $**P < 0.01$, $***P < 0.001$.

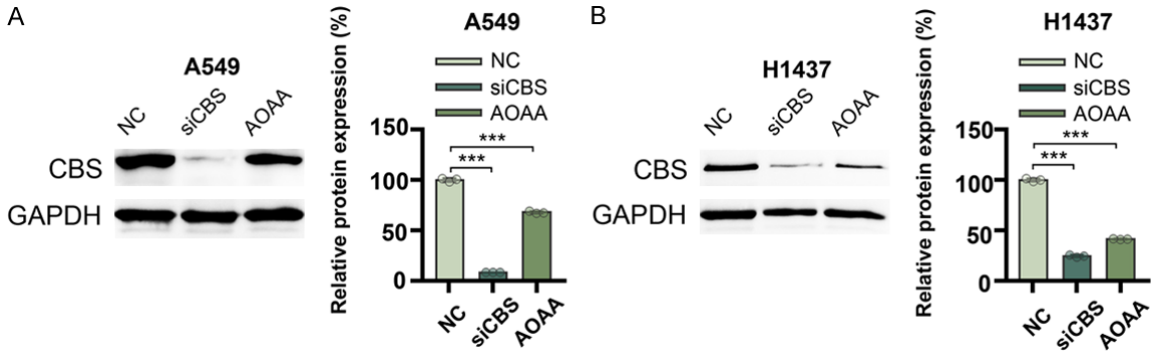

Figure S6. The expression levels of CBS in lung cancer cells with si-CBS or AOAA treatment. A. The expression levels of CBS in lung cancer cells under treatment with si-CBS or AOAA in the cells of A549. B. The expression levels of CBS in lung cancer cells under treatment with si-CBS or AOAA in the cells of H1437. Data are presented as mean ± SD, $*P < 0.05$, $**P < 0.01$, $***P < 0.001$.

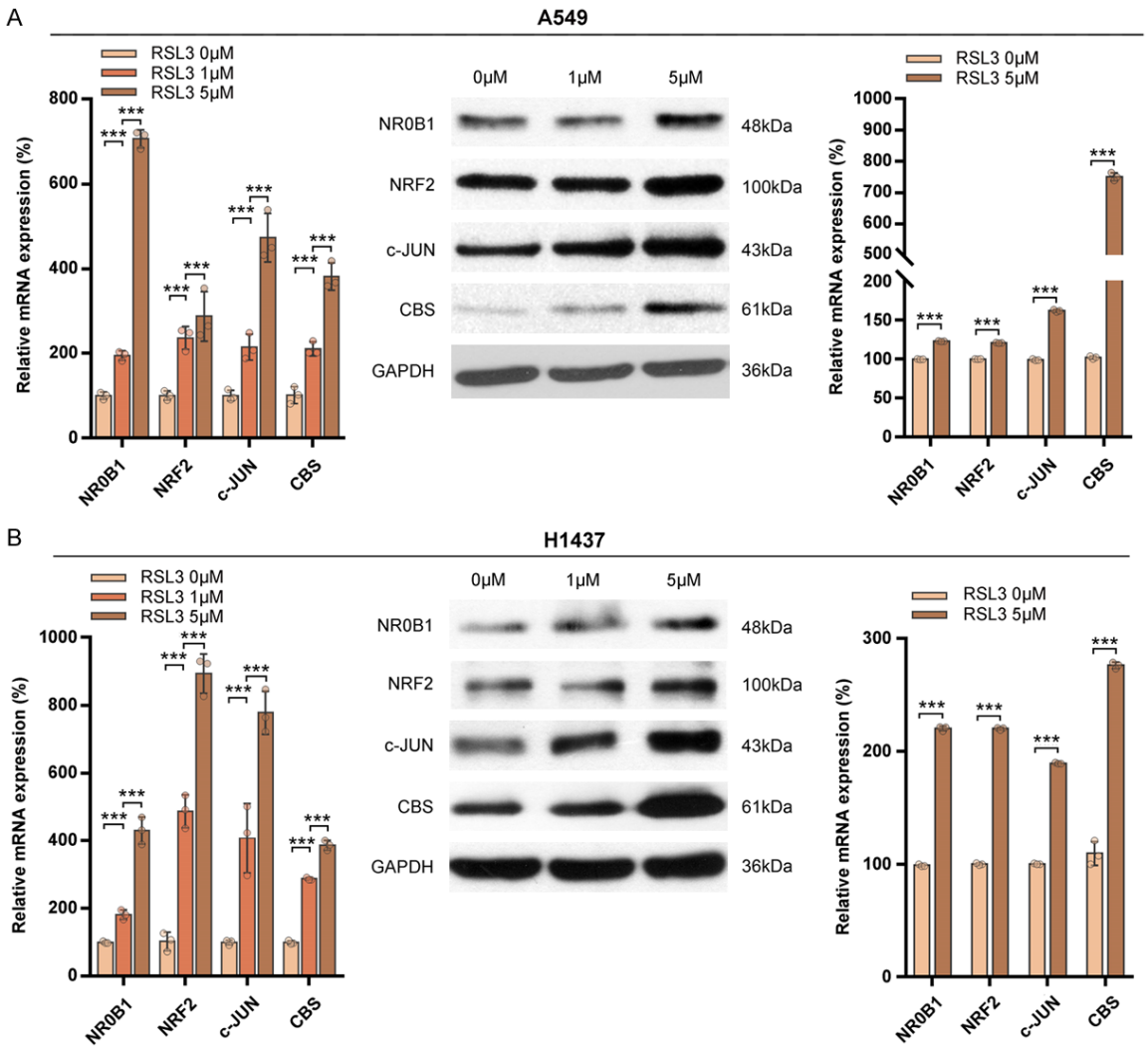

Figure S7. RSL3 activates the NR0B1 expression in lung cancer cells. A. Relative mRNA levels of *NR0B1*, *NRF2*, *c-JUN* and *CBS* in A549 and H1437 cells treated with RSL3 (0, 1, 5 μM). B. Protein levels of NR0B1, NRF2, c-JUN and CBS in A549 and H1437 cells treated with RSL3 (0, 1, 5 μM). Data are presented as mean ± SD, **P* < 0.05, ***P* < 0.01, ****P* < 0.001.